The Astronomical Journal, 145:13 (22pp), 2013 January doi:10.1088/0004-6256/145/1/13

HIGH-RESOLUTION SPECTROSCOPY OF EXTREMELY METAL-POOR STARS FROM SDSS/SEGUE. I. ATMOSPHERIC PARAMETERS AND CHEMICAL COMPOSITIONS

Wako Aoki[1,2], Timothy C. Beers[3,4], Young Sun Lee[4,13], Satoshi Honda[5], Hiroko Ito[2], Masahide Takada-Hidai[6], Anna Frebel[7], Takuma Suda[1], Masayuki Y. Fujimoto[8], Daniela Carollo[9,10,11], and Thirupathi Sivarani[12]

[1] National Astronomical Observatory, Mitaka, Tokyo 181-8588, Japan; aoki.wako@nao.ac.jp, takuma.suda@nao.ac.jp

[2] Department of Astronomical Science, School of Physical Sciences, The Graduate University of Advanced Studies (SOKENDAI), 2-21-1 Osawa, Mitaka, Tokyo 181-8588, Japan

[3] National Optical Astronomy Observatory, Tucson, AZ 85719, USA; beers@noao.edu

[4] Department of Physics & Astronomy and JINA: Joint Institute for Nuclear Astrophysics, Michigan State University, East Lansing, MI 48824, USA; lee@pa.msu.edu

[5] Kwasan Observatory, Kyoto University, Ohmine-cho Kita Kazan, Yamashin a-ku, Kyoto 607-8471, Japan; honda@kwasan.kyoto-u.ac.jp

[6] Liberal Arts Education Center, Tokai University, 4-1-1 Kitakaname, Hiratsuka, Kanagawa 259-1292, Japan; hidai@apus.rh.u-tokai.ac.jp

[7] Massachusetts Institute of Technology, Kavli Institute for Astrophysics and Space Research, 77 Massachusetts Avenue, Cambridge, MA 02139, USA; afrebel@mit.edu

[8] Department of Cosmosciences, Graduate School of Science, Hokkaido University, Kita 10 Nishi 8, Kita-ku, Sapporo 060-0810, Japan; fujimoto@astro1.sci.hokudai.ac.jp

[9] Department of Physics and Astronomy, Astronomy, Astrophysics, & Astrophotonic Research Center, Macquarie University North Ryde, NSW 2109, Australia; daniela.carollo@mq.edu.au

[10] Department of Physics & Astronomy, Macquarie University, NSW 2109, Australia

[11] INAF-Osservatorio Astronomico di Torino, Strada Osservatorio 20, Pino Torinese, I-10020, Torino, Italy

[12] Indian Institute of Astrophysics, 2nd block Koramangala, Bangalore 560034, India; sivarani@iiap.res.in

Received 2012 August 18; accepted 2012 October 2; published 2012 December 10

ABSTRACT

Chemical compositions are determined based on high-resolution spectroscopy for 137 candidate extremely metal-poor (EMP) stars selected from the Sloan Digital Sky Survey (SDSS) and its first stellar extension, the Sloan Extension for Galactic Understanding and Exploration (SEGUE). High-resolution spectra with moderate signal-to-noise (S/N) ratios were obtained with the High Dispersion Spectrograph of the Subaru Telescope. Most of the sample (approximately 80%) are main-sequence turnoff stars, including dwarfs and subgiants. Four cool main-sequence stars, the most metal-deficient such stars known, are included in the remaining sample. Good agreement is found between effective temperatures estimated by the SEGUE stellar parameter pipeline, based on the SDSS/SEGUE medium-resolution spectra, and those estimated from the broadband $(V - K)_0$ and $(g - r)_0$ colors. Our abundance measurements reveal that 70 stars in our sample have [Fe/H] < -3, adding a significant number of EMP stars to the currently known sample. Our analyses determine the abundances of eight elements (C, Na, Mg, Ca, Ti, Cr, Sr, and Ba) in addition to Fe. The fraction of carbon-enhanced metal-poor stars ([C/Fe] $> +0.7$) among the 25 giants in our sample is as high as 36%, while only a lower limit on the fraction (9%) is estimated for turnoff stars. This paper is the first of a series of papers based on these observational results. The following papers in this series will discuss the higher-resolution and higher-S/N observations of a subset of this sample, the metallicity distribution function, binarity, and correlations between the chemical composition and kinematics of extremely metal-poor stars.

Key words: Galaxy: halo – stars: abundances – stars: atmospheres – stars: Population II

Online-only material: color figures, machine-readable and VO tables

1. INTRODUCTION

The formation and evolution of the first generations of stars, once an entirely theoretical enterprise, has in recent years begun to enter the realm where observations are placing more and firmer constraints on the subject. Pertinent observations range from cosmology to star formation, stellar evolution, supernova explosions, and early galaxy formation (e.g., Bromm & Larson 2004; Ciardi & Ferrara 2005). Surveys for very high redshift galaxies, QSOs, and gamma-ray bursters have detected objects at $z \gtrsim 6$, when the age of universe was only several hundred million years. The recently reported high redshift ($z = 2.3$), extremely metal-poor damped Lyα system by Cooke et al. (2011; [Fe/H] ~ -3) exhibits enhanced carbon ([C/Fe] $= +1.5$) and other elemental abundance signatures that Kobayashi et al. (2011) associate with production by faint supernovae in the early universe.

Such studies are complemented by investigations of ancient (but still shining) stars of the Milky Way and Local Group. The elemental abundances of the chemically most primitive stars are believed to record the nucleosynthesis yields of the first generations of objects, thereby constraining their mass distribution, evolution, and nature of their supernova explosions (Beers & Christlieb 2005; Frebel & Norris 2011). If low-mass ($<0.8\ M_\odot$) stars were able to form from primordial, metal-free gas clouds, stars with zero metallicity are expected to be found in the present Galaxy.

A number of extensive searches for very metal-poor (VMP; [Fe/H] < -2) and extremely metal-poor (EMP; [Fe/H] < -3) stars in the Galaxy have been undertaken in the past few decades. Since the discovery of CD$-38°245$ with [Fe/H] ~ -4 (Bessell & Norris 1984), several objects having similar metallicity have been found by the HK survey (Beers et al. 1985, 1992) and

[13] Present address: Department of Astronomy, New Mexico State University, Las Cruces, NM 88 88003, USA.

studied with follow-up high-resolution spectroscopy. Stars with even lower metallicities have been found in recent years, including the ultra metal-poor (UMP; [Fe/H] < -4) star HE 0557-4840 (Norris et al. 2007) and the hyper metal-poor (HMP; [Fe/H] < -5) stars HE 0107-5240 (Christlieb et al. 2002) and HE 1327-2326 (Frebel et al. 2005; Aoki et al. 2006), based on follow-up observations of candidates from the Hamburg/ESO Survey (HES; Christlieb 2003; Christlieb et al. 2008), which has a fainter limiting magnitude and larger survey volume than the HK survey. Quite recently, a new UMP star with [Fe/H] ~ -5 was discovered by Caffau et al. (2011) among the candidate metal-poor stars identified with medium-resolution spectroscopy from the Sloan Digital Sky Survey (SDSS, see below).

The majority of VMP stars found by the HK survey and the HES, including the two stars with [Fe/H] < -5, are fainter than $V \sim 13$. Detailed abundance measurements, based on high-resolution spectroscopy for such stars, has only become possible through the use of 8–10 m class telescopes such as Keck, the Very Large Telescope, and Subaru. Previous studies of large samples of candidate metal-poor stars from these surveys have revealed the chemical compositions of stars with [Fe/H] ~ -3 (Cayrel et al. 2004; Cohen et al. 2004; Honda et al. 2004; Barklem et al. 2005; Aoki et al. 2005; Lai et al. 2008; Bonifacio et al. 2009). However, the sample size of stars having even lower metallicity, in particular for the intrinsically fainter main-sequence turnoff stars, is still rather small, and the relationship between the abundance patterns observed for the EMP, UMP, and HMP stars remains unclear. A large sample of candidate metal-poor stars have been provided by SDSS (see below), and abundance studies for them based on high-resolution spectroscopy have been rapidly growing (e.g., Aoki et al. 2008; Caffau et al. 2011; Bonifacio et al. 2012).[14]

In this paper, the first of a series, we report on follow-up high-resolution "snapshot" ($R \sim 36{,}000$, $30 \lesssim$ S/N $\lesssim 60$) spectroscopic observations of a large sample (137) of candidate EMP stars selected from the SDSS (York et al. 2000), and the Sloan Extension for Galactic Understanding and Exploration (SEGUE) sub-survey of the SDSS (Yanny et al. 2009). In this paper we describe the selection of our targets (Section 2), the observational and reduction/analysis procedures used (Section 3), and the determinations of stellar atmospheric parameters and estimates of a limited number of important elements (C, Na, Mg, Ca, Ti, Cr, Sr, and Ba; Section 4). In Section 4, we also comment briefly on a number of the double-lined (and one triple-lined!) spectroscopic binaries discovered during the course of this work. In Section 5, we discuss the nature of the carbon-enhanced metal-poor (CEMP) stars found in our sample, and the trends and outliers found among the α-elements and the neutron-capture elements for stars in our sample.

Papers to follow in this series will discuss constraints on the low-metallicity tail of the halo-system metallicity distribution function, the binarity properties of the sample, and correlations between the chemical compositions and kinematics of VMP and EMP stars. Results of higher-S/N, higher resolution spectroscopy of a number of the most interesting stars found during this effort will also be presented, including the Li abundances for main-sequence turnoff stars.

[14] After our work is completed, a series of papers on a large sample of metal-poor stars by Norris et al. (2012) and Yong et al. (2012) have appeared. Their sample includes some EMP stars discovered by SDSS.

2. SAMPLE SELECTION

2.1. Selection of Candidate EMP Stars from SDSS/SEGUE

SDSS-I was an imaging and spectroscopic survey that began routine operations in 2000 April, and continued through 2005 June. The SDSS, and its extensions, use a dedicated 2.5 m telescope (Gunn et al. 2006) located at the Apache Point Observatory in New Mexico. The telescope is equipped with an imaging camera and a pair of spectrographs, each of which is capable of simultaneously collecting 320 medium-resolution ($R \sim 1800$) spectra over its seven square degree field of view, so that on the order of 600 individual target spectra and roughly 40 calibration-star and sky spectra are obtained on a given spectroscopic "plug-plate." It is important to recall that SDSS imaging (done in drift-scan mode) has an effective bright limit corresponding to roughly $g \sim 14.0$–14.5, which means that high-resolution spectroscopic follow-up observations for large samples of these stars is challenging to obtain with telescopes of 4m aperture and smaller.

The SEGUE sub-survey, carried out as part of SDSS-II, ran from 2005 July to 2008 June. SEGUE obtained some 240,000 medium-resolution spectra of stars in the Galaxy, selected to explore the nature of stellar populations from 0.5 kpc to 100 kpc (Yanny et al. 2009). These stars, as well as all previous SDSS stellar observations, were released as part of DR7 (Abazajian et al. 2009).

The SEGUE Stellar Parameter Pipeline (SSPP) processes the wavelength- and flux-calibrated spectra generated by the standard SDSS spectroscopic reduction pipeline, obtains equivalent widths and/or line indices for about 80 atomic or molecular absorption lines, and estimates the effective temperature, $T_{\rm eff}$, surface gravity, $\log g$, and metallicity, [Fe/H], for a given star through the application of a number of approaches. A given method is usually optimal over specific ranges of color and S/N ratio. The SSPP employs 8 primary methods for the estimation of $T_{\rm eff}$, 10 for the estimation of $\log g$, and 12 for the estimation of [Fe/H]. The final estimates of the atmospheric parameters are obtained by robust averages of the methods that are expected to perform well for the color and S/N obtained for each star. The use of multiple methods allows for empirical determinations of the internal errors for each parameter, based on the range of reported values from each method—typical internal errors for stars in the temperature range that applies to the calibration stars are $\sigma(T_{\rm eff}) \sim 100$ K to $\sim$125 K, $\sigma(\log g) \sim 0.25$ dex, and σ([Fe/H]) ~ 0.20 dex. The external errors in these determinations are of a similar size. See Lee et al. (2008a, 2008b), Allende Prieto et al. (2008), Smolinski et al. (2011), and Lee et al. (2011) for additional discussion of the SSPP. The SSPP estimates of $T_{\rm eff}$, $\log g$, and [Fe/H] were also released as part of DR7.

2.2. Sample Selection for High-resolution Spectroscopy

In order to assemble a set of likely EMP stars for high-resolution spectroscopy with Subaru/HDS, we selected targets that have $V_0 \lesssim 16.5$ ($g_0 \lesssim 16.7$) and [Fe/H] $\leqslant -2.7$, as provided by the SSPP, in the temperature range 4500 K $< T_{\rm eff} <$ 7000 K, over which the SSPP estimates are best behaved. The choice of a conservative upper metallicity cut of [Fe/H] $= -2.7$ was made because previous high-resolution follow-up with Subaru and other telescopes had shown that the SSPP estimates of metallicity, at the time of sample selection, were consistently 0.2–0.3 dex too high at the lowest metallicities. The upper panel of Figure 1 shows the distribution of [Fe/H] estimated from SDSS spectra (horizontal axis) using the version

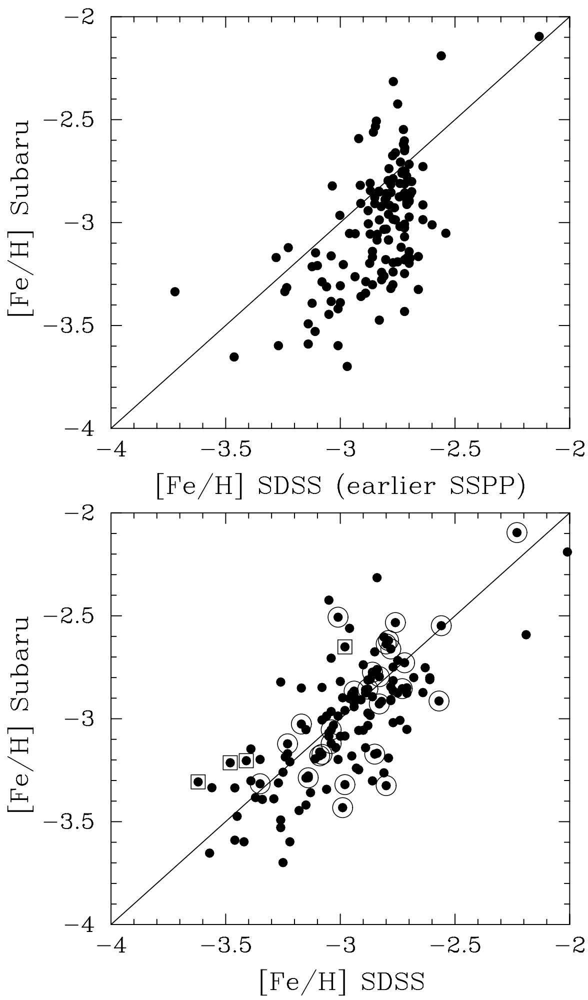

Figure 1. Upper panel: comparison of [Fe/H], based on the snapshot Subaru high-resolution spectra, with those estimated from medium-resolution SDSS spectra, based on the version of the SSPP in use prior to 2008. Lower panel: same as the upper panel, but using estimates from the latest version of the SSPP. Large open circles and squares are overplotted for giants and cool main-sequence stars, respectively. The level of improvement in the SSPP is clear.

of the SSPP that was available when the targets for Subaru/HDS observations were selected in early 2008. Several stars having higher SSPP estimates of [Fe/H] or $V_0 > 16.5$ were observed when appropriate targets did not exist in the observing period with Subaru/HDS. The Subaru high-resolution estimates of [Fe/H] for these same stars, shown on the vertical axis, are described below.

It is clear from Figure 1 that the conservative choice of metallicity cut was indeed appropriate, as a considerable fraction (65%) of the stars with high-resolution estimates of $[Fe/H] < -3.0$ would have been missed had we set the selection boundary at $[Fe/H] (SSPP) = -3.0$. The lower panel of Figure 1 shows the effect of recent improvements in the SSPP, as discussed further below (Section 4.2).

The list of 137 stars for which acceptable high-resolution spectroscopy was obtained with Subaru/HDS is given in Table 1, where the object name, coordinates, photometry, and reddening data are provided, and discussed in detail below. In the following analysis, the objects are separated into turnoff stars, giants, and cool main-sequence stars, based on determinations of their effective temperature and gravity. According to this taxonomy, about 80% of the objects in our sample are main-sequence turnoff stars. Note that although some objects were identified as carbon-rich stars from the SDSS medium-resolution spectra prior to our obtaining high-resolution follow-up spectra, we gave no preference in their choice (for or against), so that our estimates of the fractions of such stars at low metallicity remains meaningful (see below).

3. OBSERVATIONS AND DATA REDUCTION

Acceptable quality high-resolution snapshot spectra for 137 of the original 143 target stars selected above were obtained with the Subaru Telescope High Dispersion Spectrograph (HDS; Noguchi et al. 2002) in four observing runs in 2008 (March, May, July, and October). Several stars among the remaining eight stars were excluded because their S/N ratios were insufficient for our purpose. The other stars exhibit spectra that differ from "normal" metal-poor stars. The objects which are excluded in the analyses are reported in the Appendix.

The spectra cover 4000–6800 Å, with a gap of 5330–5430 Å due to the separation of the two EEV-CCDs used in the spectrograph. The resolving power $R = 36{,}000$ is obtained with the slit of 1.0 arcsec width and 2×2 CCD on-chip binning. The observing log is listed in Table 2, where the observing dates, exposure time, signal-to-noise (S/N) ratios, and heliocentric radial velocity are presented. The average S/N ratios at 4300 and 5000 Å per resolution element are 31 and 51, respectively.

Data reduction was carried out with standard procedures using the IRAF echelle package,[15] including bias-level correction using the overscan regions of the CCD data, scattered light subtraction, flat-fielding, extraction of spectra, and wavelength calibration using Th arc lines. Cosmic-ray hits were removed by the method described in Aoki et al. (2005). Sky background was not very significant in our spectra, which were obtained during times of little contamination from the moon. The multi-order echelle spectra were combined into a single spectrum by adding photon counts for the overlapping wavelength regions, and the combined spectrum was then normalized to the continuum level. Spectra obtained with more than one exposure were combined by adding photon counts before continuum normalization.

3.1. Equivalent Width Measurements

Equivalent widths (W's) were measured for isolated absorption lines in our spectra by fitting Gaussian profiles, using the line list given in Table 3. The measurements were made with a fortran program of Gaussian fitting based on Press et al. (1992), including an estimate of the continuum level around each absorption line.

The number of lines detected in the spectra depends on the metallicity, the stellar luminosity classification, and the S/N ratio. In the spectra of turnoff stars, typically 10–20 Fe I lines are measured. In some spectra with relatively lower S/N ratios and relatively high temperatures, the number of Fe I lines detected is less than 10. While a few Fe II lines are measured in most turnoff stars, no Fe II line is detected for 24 of our stars. A few lines of Na I, Mg I, and Ca I are measured for most turnoff stars, while other elements (e.g., Sc, Ti, Sr, Ba) are detected only for a limited number of objects. In general, the number of lines measured for giants is larger than that for turnoff stars, due to their lower effective temperatures. At least a few Fe II lines are detected for all giants in our sample.

[15] IRAF is distributed by the National Optical Astronomy Observatory, which is operated by the Association of Universities for Research in Astronomy, Inc. under cooperative agreement with the National Science Foundation.

Table 1
Object List

ID	Object	Object Name	Object ID	g_0	$(g-r)_0$	V_0[a]	$E(B-V)$[b]	K[c]
001	SDSS J0002 + 2928	SDSS J000219.87 + 292851.8	2803-54368-459	15.133	0.304	14.958	0.051	13.683
002	SDSS J0008−0529	SDSS J000812.54−052926.5	2624-54380-061	16.564	0.737	16.147	0.033	13.620
003	SDSS J0018−0939	SDSS J001820.51−093939.2	1912-53293-352	16.140	0.789	15.693	0.045	13.278
004	SDSS J0020−0040	SDSS J002015.45−004058.1	1121-52873-136	16.619	0.221	16.491	0.028	15.069
005	SDSS J0021−0050	SDSS J002113.78−005005.2	0390-51816-187	16.571	0.262	16.420	0.028	15.403
006	SDSS J0023−0003	SDSS J002356.26−000311.9	0688-52203-152	16.454	0.405	16.223	0.028	14.505
007	SDSS J0027 + 1404	SDSS J002749.46 + 140418.1	0753-52233-013	16.533	0.278	16.373	0.102	15.013
008	SDSS J0027−1909	SDSS J002756.76−190929.8	2848-54453-300	15.574	0.204	15.456	0.024	14.390
009	SDSS J0028−1015	SDSS J002857.42−101530.7	1912-53293-031	16.734	0.281	16.572	0.036	15.408
010	SDSS J0029−1910	SDSS J002910.72−191007.5	2848-54453-252	14.273	0.221	14.145	0.022	13.048
011	SDSS J0033−1859	SDSS J003305.15−185906.8	2848-54453-059	16.440	0.577	16.112	0.020	13.841
012	SDSS J0041−0953	SDSS J004150.22−095327.7	0656-52148-307	16.900	0.320	16.716	0.033	15.248
013	SDSS J0100 + 0049	SDSS J010026.69 + 004915.8	1083-52520-579	15.995	0.420	15.755	0.026	13.993
014	SDSS J0111 + 1442	SDSS J011150.32 + 144207.8	2804-54368-126	15.546	0.279	15.385	0.046	14.106
015	SDSS J0115 + 2637	SDSS J011501.57 + 263708.8	2040-53384-407	15.754	0.427	15.510	0.059	13.764
016	SDSS J0120−1001	SDSS J012032.63−100106.5	2849-54454-012	16.591	0.332	16.401	0.037	14.779
017	SDSS J0126 + 0607	SDSS J012617.95 + 060724.8	2314-53713-090	15.634	0.188	15.525	0.029	14.468
018	SDSS J0131−0908	SDSS J013152.01−090851.8	1914-53729-357	15.877	0.564	15.557	0.027	13.420
019	SDSS J0140 + 2344	SDSS J014036.22 + 234458.1	2044-53327-515	15.340	0.345	15.142	0.133	13.668
020	SDSS J0209 + 2120	SDSS J020912.03 + 212028.1	2046-53327-124	16.865	0.273	16.708	0.120	15.267
021	SDSS J0254 + 3328	SDSS J025453.33 + 332840.9	2378-53759-083	16.817	0.248	16.674	0.101	15.379
022	SDSS J0259 + 0057	SDSS J025956.45 + 005713.3	1513-53741-338	16.397	0.758	15.968	0.081	13.673
023	SDSS J0308 + 0505	SDSS J030839.27 + 050534.9	2335-53730-314	15.774	0.372	15.561	0.247	14.261
024	SDSS J0317 + 0023	SDSS J031745.82 + 002304.2	0711-52202-489	16.461	0.333	16.270	0.087	14.791
025	SDSS J0320 + 4143	SDSS J032044.05 + 414345.5	2397-53763-563	15.190	0.303	15.016	0.174	13.710
026	SDSS J0351 + 1026	SDSS J035111.27 + 102643.2	2679-54368-543	16.062	0.340	15.867	0.234	14.283
027	SDSS J0414 + 0552	SDSS J041438.25 + 055219.8	2805-54380-301	15.973	0.203	15.855	0.317	14.973
028	SDSS J0416 + 0713	SDSS J041618.03 + 071303.4	2805-54380-329	16.432	0.509	16.142	0.398	14.499
029	SDSS J0629 + 8303	SDSS J062947.45 + 830328.6	2540-54110-062	15.633	0.455	15.374	0.069	13.663
030	SDSS J0630 + 2552	SDSS J063055.58 + 255243.7	2696-54167-214	16.839	0.274	16.681	0.327	15.968
031	SDSS J0711 + 6702	SDSS J071105.43 + 670228.2	2337-53740-564	16.046	0.494	15.765	0.053	13.860
032	SDSS J0723 + 3637	SDSS J072352.21 + 363757.2	2941-54507-222	15.302	0.540	14.995	0.061	12.903
033	SDSS J0727 + 1609	SDSS J072725.15 + 160949.4	2713-54400-390	15.816	0.255	15.669	0.087	14.305
034	SDSS J0741 + 6708	SDSS J074104.22 + 670801.8	2939-54515-414	15.626	0.539	15.320	0.040	13.313
035	SDSS J0746 + 2831	SDSS J074641.34 + 283142.7	1059-52618-429	15.906	0.305	15.731	0.033	14.442
036	SDSS J0748 + 1758	SDSS J074859.89 + 175832.8	1921-53317-334	15.727	0.276	15.568	0.051	14.285
037	SDSS J0749 + 1801	SDSS J074945.24 + 180103.6	2054-53431-033	14.603	0.569	14.292	0.054	12.186
038	SDSS J0804 + 5153	SDSS J080428.21 + 515303.1	1870-53383-002	16.267	0.342	16.071	0.055	14.451
039	SDSS J0809 + 0907	SDSS J080917.06 + 090748.5	2419-54139-037	16.068	0.268	15.914	0.021	14.607
040	SDSS J0814 + 3337	SDSS J081458.68 + 333712.9	0825-52289-595	16.208	0.216	16.083	0.050	14.928
041	SDSS J0817 + 2641	SDSS J081754.93 + 264103.8	1266-52709-432	16.179	0.290	16.012	0.037	14.707
042	SDSS J0819 + 3119	SDSS J081923.99 + 311919.4	0931-52619-469	16.085	0.233	15.950	0.038	14.730
043	SDSS J0821 + 1819	SDSS J082118.18 + 181931.8	2271-53726-365	16.602	0.262	16.451	0.037	15.101
044	SDSS J0825 + 0403	SDSS J082521.29 + 040334.4	1185-52642-519	16.965	0.221	16.837	0.027	15.182
045	SDSS J0827 + 1052	SDSS J082736.27 + 105200.8	2423-54149-031	16.519	0.237	16.382	0.045	15.057
046	SDSS J0840 + 5405	SDSS J084016.16 + 540526.5	0446-51899-239	16.265	0.253	16.119	0.026	14.533
047	SDSS J0847 + 0121	SDSS J084700.50 + 012113.7	0467-51901-484	15.595	0.226	15.464	0.044	14.123
048	SDSS J0851 + 1018	SDSS J085136.68 + 101803.2	2667-54142-094	15.099	0.254	14.953	0.054	13.731
049	SDSS J0858 + 3541	SDSS J085833.35 + 354127.3	2380-53759-094	15.301	0.583	14.970	0.031	12.933
050	SDSS J0859 + 0402	SDSS J085934.48 + 040232.4	2888-54529-615	15.994	0.498	15.711	0.046	13.766
051	SDSS J0907 + 0246	SDSS J090733.28 + 024608.1	0566-52238-100	16.256	0.299	16.084	0.029	14.784
052	SDSS J0912 + 0216	SDSS J091243.72 + 021623.7	0471-51924-613	15.560	0.324	15.374	0.028	14.065
053	SDSS J0932 + 0241	SDSS J093247.29 + 024123.8	0475-51965-602	16.378	0.229	16.246	0.049	14.752
054	SDSS J1004 + 3442	SDSS J100427.70 + 344245.7	2387-53770-316	14.795	0.297	14.624	0.010	13.185
055	SDSS J1033 + 4001	SDSS J103301.41 + 400103.6	1430-53002-498	16.118	0.217	15.992	0.014	14.701
056	SDSS J1036 + 1212	SDSS J103649.93 + 121219.8	1600-53090-378	15.580	0.332	15.390	0.027	13.817
057	SDSS J1106 + 0343	SDSS J110610.48 + 034321.9	0581-52356-245	16.463	0.274	16.305	0.058	15.324
058	SDSS J1108 + 1747	SDSS J110821.68 + 174746.6	2491-53855-389	15.702	0.308	15.525	0.022	14.177
059	SDSS J1120 + 3027	SDSS J112051.74 + 302724.4	1979-53431-181	16.011	0.391	15.788	0.015	14.224
060	SDSS J1128 + 3841	SDSS J112813.57 + 384148.9	2036-53446-324	15.523	0.197	15.408	0.022	14.256
061	SDSS J1147 + 1510	SDSS J114723.53 + 151044.7	1761-53376-551	16.118	0.218	15.992	0.049	14.956
062	SDSS J1159 + 5425	SDSS J115906.18 + 542512.6	1018-52672-268	16.145	0.383	15.926	0.012	14.405
063	SDSS J1213 + 4450	SDSS J121307.22 + 445040.9	1370-53090-458	16.176	0.167	16.078	0.013	14.741
064	SDSS J1230 + 0005	SDSS J123055.25 + 000546.9	2895-54565-360	14.701	0.256	14.553	0.027	13.182
065	SDSS J1233 + 3407	SDSS J123300.08 + 340758.1	2020-53431-313	16.734	0.285	16.570	0.018	15.206
066	SDSS J1241−0837	SDSS J124123.92−083725.5	2689-54149-292	16.309	0.603	15.967	0.028	13.788

Table 1
(Continued)

ID	Object	Object Name	Object ID	g_0	$(g-r)_0$	V_0[a]	$E(B-V)$[b]	K[c]
067	SDSS J1242−0336	SDSS J124204.42−033618.1	2897-54585-210	14.661	0.550	14.348	0.024	12.217
068	SDSS J1245−0738	SDSS J124502.68−073847.1	2689-54149-491	16.230	0.283	16.067	0.029	14.815
069	SDSS J1300 + 2632	SDSS J130017.20 + 263238.6	2240-53823-008	16.180	0.233	16.045	0.008	14.839
070	SDSS J1303 + 2515	SDSS J130339.62 + 251550.3	2662-54505-455	15.741	0.282	15.579	0.011	14.287
071	SDSS J1304 + 3239	SDSS J130402.25 + 323909.1	2029-53819-374	16.522	0.244	16.381	0.009	15.186
072	SDSS J1312 + 2450	SDSS J131201.48 + 245007.0	2663-54234-467	15.730	0.271	15.574	0.015	14.155
073	SDSS J1316 + 1747	SDSS J131640.80 + 174734.2	2476-53826-575	15.587	0.743	15.166	0.000	12.688
074	SDSS J1334 + 0022	SDSS J133453.44 + 002238.6	0298-51955-485	15.949	0.403	15.719	0.026	14.025
075	SDSS J1338 + 1204	SDSS J133841.16 + 120415.2	1700-53502-483	15.613	0.267	15.459	0.026	14.230
076	SDSS J1349−0229	SDSS J134913.54−022942.8	0913-52433-073	16.462	0.296	16.292	0.045	14.688
077	SDSS J1400 + 0753	SDSS J140035.31 + 075317.7	1807-54175-089	16.735	0.255	16.588	0.026	15.070
078	SDSS J1408 + 6239	SDSS J140813.88 + 623942.1	0605-52353-567	16.624	0.242	16.484	0.022	15.242
079	SDSS J1410 + 5350	SDSS J141001.77 + 535018.2	1325-52762-194	16.171	0.271	16.015	0.012	14.761
080	SDSS J1412 + 5609	SDSS J141207.32 + 560931.9	2447-54498-274	15.949	0.139	15.867	0.014	14.622
081	SDSS J1422 + 0031	SDSS J142237.43 + 003105.2	0304-51609-528	16.505	0.304	16.330	0.030	14.120
082	SDSS J1424 + 5615	SDSS J142441.88 + 561535.0	2447-54498-073	15.788	0.257	15.640	0.015	14.168
083	SDSS J1425 + 1137	SDSS J142518.09 + 113713.9	1708-53503-250	15.628	0.236	15.492	0.027	14.191
084	SDSS J1425 + 5742	SDSS J142541.33 + 574207.5	2539-53918-264	16.231	0.194	16.118	0.009	14.836
085	SDSS J1434 + 1036	SDSS J143451.02 + 103626.4	1709-53533-595	16.926	0.245	16.785	0.025	14.959
086	SDSS J1436 + 0918	SDSS J143632.27 + 091831.5	1711-53535-285	15.958	0.233	15.823	0.030	14.784
087	SDSS J1436 + 0301	SDSS J143654.45 + 030143.2	0536-52024-405	16.982	0.276	16.823	0.034	15.399
088	SDSS J1437 + 5231	SDSS J143708.92 + 523146.6	1327-52781-480	16.265	0.243	16.125	0.010	14.906
089	SDSS J1437 + 5837	SDSS J143759.06 + 583723.5	0790-52433-535	15.809	0.243	15.669	0.008	14.442
090	SDSS J1446 + 1249	SDSS J144640.63 + 124917.5	1712-53531-636	16.084	0.239	15.946	0.021	14.505
091	SDSS J1502 + 3113	SDSS J150217.16 + 311316.5	2910-54630-287	15.662	0.222	15.533	0.018	14.282
092	SDSS J1504 + 4623	SDSS J150425.13 + 462320.9	1049-52751-126	16.526	0.267	16.372	0.018	15.025
093	SDSS J1515 + 4503	SDSS J151534.44 + 450317.7	1050-52721-132	16.491	0.286	16.327	0.032	15.129
094	SDSS J1516 + 4333	SDSS J151646.69 + 433331.6	1677-53148-588	16.613	0.191	16.502	0.022	15.328
095	SDSS J1521 + 3437	SDSS J152158.62 + 343729.4	1354-52814-191	16.828	0.290	16.661	0.020	15.458
096	SDSS J1522 + 3055	SDSS J152202.09 + 305526.3	1650-53174-492	16.518	0.334	16.327	0.022	14.802
097	SDSS J1523 + 4942	SDSS J152301.86 + 494210.7	2449-54271-200	15.828	0.361	15.621	0.022	14.041
098	SDSS J1528 + 4915	SDSS J152810.51 + 491526.8	2449-54271-142	15.492	0.199	15.376	0.017	14.161
099	SDSS J1551 + 2521	SDSS J155117.36 + 252135.5	1850-53786-467	16.129	0.322	15.944	0.060	14.448
100	SDSS J1553 + 2511	SDSS J155310.83 + 251140.2	2459-54339-140	16.387	0.389	16.165	0.062	14.544
101	SDSS J1603 + 2917	SDSS J160303.74 + 291709.5	1578-53496-471	16.519	0.291	16.352	0.040	15.122
102	SDSS J1612 + 0421	SDSS J161226.18 + 042146.6	2178-54629-546	16.082	0.449	15.826	0.069	14.053
103	SDSS J1613 + 5309	SDSS J161313.53 + 530909.7	2176-54243-614	16.658	0.470	16.390	0.013	14.402
104	SDSS J1623 + 3913	SDSS J162311.84 + 391319.6	1172-52759-319	16.448	0.268	16.294	0.010	15.120
105	SDSS J1626 + 1458	SDSS J162603.61 + 145844.3	2202-53566-537	16.998	0.232	16.864	0.056	15.371
106	SDSS J1633 + 3907	SDSS J163331.44 + 390742.7	1173-52790-561	16.743	0.277	16.584	0.009	14.951
107	SDSS J1640 + 3709	SDSS J164005.30 + 370907.8	2174-53521-423	15.622	0.240	15.483	0.016	14.191
108	SDSS J1646 + 2824	SDSS J164610.19 + 282422.2	1690-53475-323	15.806	0.314	15.626	0.065	14.451
109	SDSS J1650 + 2242	SDSS J165016.66 + 224213.9	2180-54613-258	16.145	0.242	16.005	0.063	14.898
110	SDSS J1659 + 3515	SDSS J165934.74 + 351554.3	0974-52427-332	16.586	0.266	16.433	0.019	14.974
111	SDSS J1703 + 2836	SDSS J170339.60 + 283649.9	2808-54524-510	15.679	0.593	15.342	0.065	13.271
112	SDSS J1728 + 0657	SDSS J172846.88 + 065701.9	2797-54616-258	16.260	0.247	16.117	0.116	15.088
113	SDSS J1734 + 4316	SDSS J173417.89 + 431606.5	2799-54368-138	16.499	0.547	16.188	0.026	14.273
114	SDSS J1735 + 4446	SDSS J173532.16 + 444635.9	2799-54368-502	15.910	0.545	15.600	0.021	13.391
115	SDSS J1736 + 4420	SDSS J173628.07 + 442036.2	2799-54368-560	16.141	0.497	15.858	0.022	13.894
116	SDSS J1746 + 2455	SDSS J174624.13 + 245548.8	2183-53536-175	16.022	0.521	15.726	0.064	13.665
117	SDSS J1830 + 4141	SDSS J183045.75 + 414126.8	2798-54397-354	15.939	0.183	15.832	0.057	14.670
118	SDSS J1834 + 2023	SDSS J183414.28 + 202335.5	2534-53917-002	16.277	0.184	16.170	0.204	14.984
119	SDSS J1836 + 6317	SDSS J183601.71 + 631727.4	2552-54632-090	16.345	0.569	16.022	0.052	14.326
120	SDSS J2005−1045	SDSS J200513.48−104503.2	2303-54629-377	16.477	0.234	16.342	0.138	15.101
121	SDSS J2052 + 0109	SDSS J205252.68 + 010939.3	2815-54414-098	16.890	0.311	16.712	0.096	15.380
122	SDSS J2104−0104	SDSS J210454.84−010440.8	1918-53240-306	16.579	0.479	16.306	0.066	14.482
123	SDSS J2111 + 0109	SDSS J211125.40 + 010920.4	1112-53180-325	16.461	0.256	16.313	0.102	15.008
124	SDSS J2118−0640	SDSS J211850.12−064055.8	2305-54414-429	16.364	0.235	16.228	0.154	15.117
125	SDSS J2123−0820	SDSS J212310.83−082039.1	2305-54414-081	16.716	0.319	16.533	0.074	15.152
126	SDSS J2128−0756	SDSS J212841.25−075629.3	0641-52199-315	16.479	0.268	16.325	0.062	14.832
127	SDSS J2206−0925	SDSS J220646.20−092545.7	2309-54441-290	15.227	0.571	14.903	0.034	12.735
128	SDSS J2207 + 2017	SDSS J220743.35 + 201752.3	2251-53557-279	16.782	0.212	16.659	0.070	15.468
129	SDSS J2208 + 0613	SDSS J220845.57 + 061341.3	2308-54379-227	15.549	0.251	15.404	0.119	14.192
130	SDSS J2213−0726	SDSS J221334.14−072604.1	2309-54441-564	15.326	0.643	14.961	0.051	12.636
131	SDSS J2300 + 0559	SDSS J230026.35 + 055956.2	2310-53710-131	16.341	0.245	16.200	0.073	14.914
132	SDSS J2308−0855	SDSS J230814.85−085526.4	0726-52226-335	16.347	0.313	16.167	0.041	15.137

Table 1
(Continued)

ID	Object	Object Name	Object ID	g_0	$(g-r)_0$	V_0[a]	$E(B-V)$[b]	K[c]
133	SDSS J2309+2308	SDSS J230959.55+230803.0	2623-54096-458	16.446	0.335	16.254	0.230	14.884
134	SDSS J2334+1538	SDSS J233403.22+153829.3	0747-52234-337	16.011	0.229	15.879	0.076	14.698
135	SDSS J2338+0902	SDSS J233817.55+090207.5	2622-54095-483	15.099	0.774	14.661	0.128	12.192
136	SDSS J2349+3832	SDSS J234939.71+383217.8	1882-53262-132	16.312	0.200	16.196	0.189	14.802
137	SDSS J2357−0052	SDSS J235718.91−005247.8	1489-52991-251	15.959	0.612	15.612	0.030	13.567

Notes.
[a] V_0 is derived by the transform of Zhao & Newberg (2006).
[b] $E(B-V)$ is estimated from Schlegel et al. (1998).
[c] K is taken from 2MASS (Skrutskie et al. 2006).

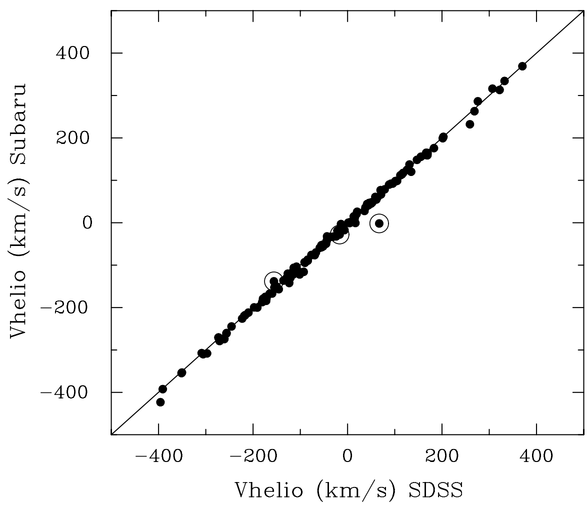

Figure 2. Comparison of heliocentric radial velocities measured from the Subaru spectra with those from SDSS spectra. The open circles are overplotted for the three double-lined spectroscopic binaries. Except for these three stars, the two measurements exhibit excellent agreement.

3.2. Radial Velocities

Radial velocities are measured using the Fe I lines for which equivalent widths are measured. The derived heliocentric radial velocities are given in Table 2. The random error in the measurement is estimated to be $\sigma_v N^{-1/2}$, where σ_v is the standard deviation of the derived values from individual lines, and N is the number of lines used. The table also provides the values obtained from the SDSS spectra used for sample selection. Comparisons of heliocentric radial velocities measured from the Subaru spectra with those from SDSS are shown in Figure 2. In our sample, three double-lined spectroscopic binaries are included, as reported below. The data points of these stars are overplotted by open circles in the figure. Excluding these stars, the agreement between the two measurements is quite good, in almost all cases well within the expected errors.

4. ABUNDANCE ANALYSIS

4.1. Effective Temperature Estimates

Chemical abundances are determined by a standard analysis for measured equivalent widths using the ATLAS NEWODF grid of model atmospheres, assuming no convective overshooting (Castelli & Kurucz 2003). The calculations of equivalent widths from models are made by the LTE spectrum synthesis code based on the programs for the model atmospheres developed by Tsuji (1978).

Owing to the lack of sufficient numbers of well-measured metallic lines in our snapshot spectra, we are not in a position to determine spectroscopic estimates of $T_{\rm eff}$ by the usual practice of minimizing the trend of the relationship between derived abundance and excitation potentials of the lines from which it is derived. Balmer line profiles are also not used to determine $T_{\rm eff}$, because the S/N ratios of our data are too low for accurate estimation of the continuum levels, although the Balmer lines were used in the first inspection of stellar types (see also the Appendix). Instead, we have first estimated effective temperatures based on two sets of color indices (Table 4), an approach that also has limitations. For example, estimates of $T_{\rm eff}$ derived for stars affected by large reddening are more uncertain, due to errors in obtaining estimates of their intrinsic colors.

Estimates of effective temperature based on $(V-K)_0$ colors are made using the temperature scales of Casagrande et al. (2010) for turnoff stars ($T_{\rm eff\,SSPP} \geqslant 5500$ K), and Alonso et al. (1999) for giants ($T_{\rm eff\,SSPP} < 5500$ K). The metallicity is assumed to be [Fe/H] $= -3.0$ for all stars in order to carry out this calculation. The V_0 magnitude is derived from the SDSS g_0 and $(g-r)_0$, using the transformations of Zhao & Newberg (2006), which are suitable for low-metallicity stars. The K_0 magnitude is adopted from the Two Micron All Sky Survey (2MASS) catalog (Skrutskie et al. 2006). In all cases, the absorption and reddening corrections were carried out based on the reddening estimates from Schlegel et al. (1998).

The top panel of Figure 3 shows a comparison of $T_{\rm eff}$ between the estimate from $(V-K)_0$ and that supplied by the SSPP. The SSPP actually provides two sets of effective temperature estimates, one of which is based on spectroscopy alone (essentially relying on the shape of the calibrated spectral energy distribution, index measurements of temperature-sensitive lines, and spectral fitting), while the other additionally includes photometric information in the estimates. For the stars in our sample, we found essentially no zero-point offsets between these approaches, with an rms variation of no more than 50 K. Hence, we adopt the spectroscopy-only values determined by the SSPP for our comparisons. Stars for which the $T_{\rm eff}$ estimates from photometry are potentially very uncertain, due to large reddening corrections, are excluded from this comparison.

By inspection of the top panel from Figure 3, there is no significant offset between the two estimates for turnoff stars ($T_{\rm eff} \gtrsim 5500$ K), although the scatter is rather large. A likely cause of this scatter is the error in the K apparent magnitude measured by 2MASS, which can become large for stars as faint as some in our sample. An error of 0.1 mag in $(V-K)_0$ results in a $T_{\rm eff}$ error of about 200 K. The 1σ errors on the K magnitude for some of our fainter turnoff stars ($K > 14.5$) are even larger than 0.1 mag. To draw attention to these, they are shown as

Table 2
Observing Log

ID	Object	Obs. Date (1)	Obs. Date (2)	Exp. Time (minute)	S/N (4300 Å)	S/N (5180 Å)	$V_{\rm H}$ (km s^{-1})	$\sigma(V_{\rm H})$ (km s^{-1})	$V_{\rm H}^{\rm SDSS}$ (km s^{-1})
001	SDSS J0002+2928	July 6, 2008		20	40	65	−308.22	0.18	−297.2
002	SDSS J0008−0529	October 4, 2008		25	24	46	117.18	0.07	117.5
003	SDSS J0018−0939	July 5, 2008		20	26	51	−122.89	0.07	−119.9
004	SDSS J0020−0040	October 5, 2008		40	35	54	3.29	0.13	11.2
005	SDSS J0021−0050	July 5, 2008		30	32	49	−94.57	0.19	−90.2
006	SDSS J0023−0003	October 4, 2008		25	28	46	89.84	0.10	88.0
007	SDSS J0027+1404	October 5, 2008		40	31	51	27.74	0.24	35.9
008	SDSS J0027−1909	July 5, 2008	July 6, 2008	40	54	83	14.97	0.10	15.0
009	SDSS J0028−1015	October 6, 2008		40	33	52	−25.29	0.13	−19.4
010	SDSS J0029−1910	July 5, 2008		5	38	58	48.00	0.08	52.5
011	SDSS J0033−1859	October 4, 2008		25	26	47	262.89	0.08	268.6
012	SDSS J0041−0953	October 6, 2008		40	29	46	98.22	0.13	101.2
013	SDSS J0100+0049	July 6, 2008		30	38	62	48.19	0.07	51.2
014	SDSS J0111+1442	July 6, 2008		25	38	61	−130.55	0.14	−121.2
015	SDSS J0115+2637	July 4, 2008		10	25	39	−113.11	0.19	−114.8
016	SDSS J0120−1001[a]	August 22, 2008		30	28	45	−59.23	0.15	−58.7
017	SDSS J0126+0607	July 6, 2008		25	41	64	−274.31	0.16	−260.6
018	SDSS J0131−0908	August 22, 2008		25	34	61	124.57	0.08	125.8
019	SDSS J0140+2344[a]	July 5, 2008		10	28	46	−200.17	0.17	−191.0
020	SDSS J0209+2120	October 6, 2008		40	26	42	−3.12	0.42	−13.8
021	SDSS J0254+3328	October 6, 2008		40	29	46	−218.09	0.12	−216.7
022	SDSS J0259+0057	October 6, 2008		25	24	43	35.71	0.53	37.9
023	SDSS J0308+0505	August 22, 2008		15	19	35	316.08	0.25	306.7
024	SDSS J0317+0023	August 22, 2008		30	28	47	113.87	0.25	115.0
025	SDSS J0320+4143	August 22, 2008		18	30	52	−115.91	0.21	−92.8
026	SDSS J0351+1026	August 22, 2008		16	17	31	98.68	0.33	104.9
027	SDSS J0414+0552	August 22, 2008		25	19	32	97.79	0.40	102.2
028	SDSS J0416+0713	October 5, 2008		25	15	28	232.15	0.36	259.0
029	SDSS J0629+8303	October 5, 2008		15	28	50	−122.08	0.17	−101.3
030	SDSS J0630+2552	October 6, 2008		40	17	30	45.55	0.66	49.3
031	SDSS J0711+6702	October 5, 2008		20	30	53	111.79	0.08	111.8
032	SDSS J0723+3637	October 6, 2008		15	32	58	−51.69	0.12	−51.7
033	SDSS J0727+1609	October 5, 2008		20	31	51	−113.25	0.23	−105.3
034	SDSS J0741+6708	October 6, 2008		15	28	48	−167.12	0.08	−159.6
035	SDSS J0746+2831	October 5, 2008		20	34	55	−32.32	0.08	−43.4
036	SDSS J0748+1758	October 5, 2008		15	31	49	−120.97	0.10	−121.3
037	SDSS J0749+1801	October 6, 2008		10	39	72	54.57	0.05	60.9
038	SDSS J0804+5153	March 10, 2008		25	30	48	−260.21	0.10	−256.1
039	SDSS J0809+0907	March 8, 2008		25	35	54	164.78	0.26	166.4
040	SDSS J0814+3337	March 10, 2008		25	34	52	148.19	0.20	146.9
041	SDSS J0817+2641	March 10, 2008		20	32	49	−1.82	0.53	67.1
042	SDSS J0819+3119	October 5, 2008		20	31	49	369.05	0.13	370.1
043	SDSS J0821+1819	March 8, 2008		35	28	44	164.40	2.12	169.4
044	SDSS J0825+0403	March 8, 2008		40	29	45	10.90	0.73	15.1
045	SDSS J0827+1052	March 8, 2008		35	35	52	158.97	0.28	169.1
046	SDSS J0840+5405	March 10, 2008		25	34	52	−10.85	0.15	−11.0
047	SDSS J0847+0121	March 8, 2008		15	30	47	199.27	0.15	201.5
048	SDSS J0851+1018	October 6, 2008		15	39	62	45.17	0.15	50.0
049	SDSS J0858+3541	October 6, 2008		15	37	64	−226.15	0.04	−223.0
050	SDSS J0859+0402	October 6, 2008		20	28	48	155.50	0.08	155.2
051	SDSS J0907+0246	March 8, 2008		25	33	52	313.15	0.15	321.9
052	SDSS J0912+0216	October 6, 2008		15	34	54	137.18	0.13	131.1
053	SDSS J0932+0241	March 8, 2008		30	33	51	286.30	0.22	275.8
054	SDSS J1004+3442	March 10, 2008		15	55	84	−57.92	0.05	−55.0
055	SDSS J1033+4001	March 10, 2008		20	34	51	−133.14	0.18	−130.8
056	SDSS J1036+1212[a]	March 8, 2008		15	35	55	−33.54	0.13	−36.6
057	SDSS J1106+0343	March 8, 2008		30	33	51	159.79	0.13	165.4
058	SDSS J1108+1747	March 8, 2008		15	34	52	−27.93	0.55	−16.7
059	SDSS J1120+3027	March 10, 2008		15	30	47	47.53	0.12	50.6
060	SDSS J1128+3841	July 5, 2008		15	38	58	−15.88	0.39	−12.8
061	SDSS J1147+1510	May 2, 2008		36	34	52	60.81	0.12	58.8
062	SDSS J1159+5425	March 10, 2008		20	32	51	175.86	0.17	182.9
063	SDSS J1213+4450	March 10, 2008		25	37	56	92.36	0.25	95.7
064	SDSS J1230+0005	July 5, 2008		10	37	55	42.61	0.19	42.4
065	SDSS J1233+3407	July 4, 2008		40	35	55	−261.31	0.20	−256.2

Table 2
(Continued)

ID	Object	Obs. Date (1)	Obs. Date (2)	Exp. Time (minute)	S/N (4300 Å)	S/N (5180 Å)	$V_{\rm H}$ (km s^{-1})	$\sigma(V_{\rm H})$ (km s^{-1})	$V_{\rm H}^{\rm SDSS}$ (km s^{-1})
066	SDSS J1241−0837	July 6, 2008		20	28	48	334.23	0.11	332.3
067	SDSS J1242−0336	July 6, 2008		10	41	71	92.14	0.06	92.0
068	SDSS J1245−0738	March 10, 2008		20	27	42	76.88	0.27	69.9
069	SDSS J1300+2632	July 5, 2008		25	42	63	−76.45	0.50	−69.4
070	SDSS J1303+2515	July 6, 2008		20	39	61	44.13	0.13	41.5
071	SDSS J1304+3239	July 4, 2008		30	32	51	1.07	0.11	4.7
072	SDSS J1312+2450	May 2, 2008		25	28	43	−93.14	0.20	−90.9
073	SDSS J1316+1747	July 6, 2008		15	34	62	41.14	0.05	44.3
074	SDSS J1334+0022	May 2, 2008		30	35	59	−56.30	0.10	−52.6
075	SDSS J1338+1204	May 2, 2008		30	43	67	−219.57	0.11	−218.6
076	SDSS J1349−0229	July 5, 2008		25	28	44	120.21	0.51	134.7
077	SDSS J1400+0753	July 6, 2008		35	29	45	202.47	0.22	202.9
078	SDSS J1408+6239	July 4, 2008		30	32	48	46.58	0.24	45.7
079	SDSS J1410+5350	March 8, 2008		25	37	56	−138.23	0.28	−155.8
080	SDSS J1412+5609	July 6, 2008		20	34	52	−53.09	0.11	−55.3
081	SDSS J1422+0031	July 5, 2008		40	33	59	−120.20	0.11	−126.4
082	SDSS J1424+5615[a]	July 6, 2008		20	37	57	−0.83	0.12	4.5
083	SDSS J1425+1137	March 8, 2008		15	35	54	−89.63	0.10	−84.2
084	SDSS J1425+5742	March 8, 2008		30	39	60	−0.61	0.18	16.6
085	SDSS J1434+1036	July 5, 2008		40	30	46	66.60	0.32	70.9
086	SDSS J1436+0918	March 8, 2008		20	36	54	−114.55	0.24	−111.9
087	SDSS J1436+0301	July 5, 2008		40	26	42	−152.78	0.33	−151.5
088	SDSS J1437+5231	March 10, 2008		25	32	49	59.50	0.10	63.0
089	SDSS J1437+5837	March 8, 2008		20	39	59	−55.10	0.19	−53.5
090	SDSS J1446+1249	March 8, 2008		25	38	59	−106.31	0.11	−113.8
091	SDSS J1502+3113	July 6, 2008		20	39	61	−278.96	0.11	−270.8
092	SDSS J1504+4623	May 2, 2008		40	33	52	−70.13	0.28	−66.9
093	SDSS J1515+4503	March 10, 2008		25	29	45	−25.91	0.30	−20.1
094	SDSS J1516+4333	July 4, 2008		30	32	47	−152.69	0.27	−154.8
095	SDSS J1521+3437	May 2, 2008		41	30	46	−32.23	0.40	−23.9
096	SDSS J1522+3055[a]	March 8, 2008		30	34	54	−354.61	0.21	−351.3
097	SDSS J1523+4942	July 6, 2008		20	31	50	−12.94	0.20	−13.7
098	SDSS J1528+4915	March 8, 2008		15	34	53	−49.60	0.10	−45.3
099	SDSS J1551+2521	May 2, 2008		30	35	57	−122.44	0.17	−115.4
100	SDSS J1553+2511	July 4, 2008		25	30	47	−187.28	0.25	−180.6
101	SDSS J1603+2917	March 8, 2008		30	32	50	−103.75	0.11	−108.0
102	SDSS J1612+0421	October 6, 2008		20	25	43	20.40	0.11	19.1
103	SDSS J1613+5309	July 4, 2008		30	30	49	−0.01	0.16	1.5
104	SDSS J1623+3913	July 4, 2008		30	33	52	−76.18	0.32	−76.5
105	SDSS J1626+1458	July 5, 2008		40	28	43	25.83	0.56	20.4
106	SDSS J1633+3907	July 4, 2008		40	34	52	−179.27	0.13	−178.8
107	SDSS J1640+3709[a]	March 10, 2008		10	29	44	−51.14	0.25	−48.6
108	SDSS J1646+2824	July 4, 2008		15	29	46	−18.72	0.16	−21.4
109	SDSS J1650+2242	October 6, 2008		25	30	48	−33.08	0.29	−30.9
110	SDSS J1659+3515	July 4, 2008		30	30	47	−42.49	0.07	−44.1
111	SDSS J1703+2836[a]	July 6, 2008		10	24	42	−174.90	0.19	−174.0
112	SDSS J1728+0657	October 6, 2008		25	25	40	−353.37	0.22	−350.4
113	SDSS J1734+4316	October 4, 2008		25	28	49	−211.93	0.09	−209.7
114	SDSS J1735+4446	May 2, 2008		20	30	54	−142.26	0.06	−123.4
115	SDSS J1736+4420	October 4, 2008		20	30	51	−310.09	0.08	−305.5
116	SDSS J1746+2455	March 10, 2008		15	27	44	78.69	0.22	78.6
117	SDSS J1830+4141	May 2, 2008		26	35	54	−270.97	0.23	−273.2
118	SDSS J1834+2023	October 5, 2008		25	23	38	−17.45	0.22	−6.4
119	SDSS J1836+6317	October 4, 2008		20	23	45	−423.25	0.22	−395.9
120	SDSS J2005−1045[a]	July 5, 2008	July 6, 2008	60	40	62	−55.60	0.35	−51.7
121	SDSS J2052+0109	October 5, 2008		40	28	45	−184.23	0.12	−172.3
122	SDSS J2104−0104	July 5, 2008		30	29	47	−110.55	0.16	−112.5
123	SDSS J2111+0109	August 22, 2008		30	25	41	−270.65	0.16	−273.0
124	SDSS J2118−0640	August 22, 2008		30	26	43	−199.71	0.83	−197.7
125	SDSS J2123−0820	July 5, 2008		40	34	51	−167.33	0.19	−164.8
126	SDSS J2128−0756	October 5, 2008		30	30	48	−178.24	0.11	−171.5
127	SDSS J2206−0925	July 4, 2008		15	41	71	14.85	0.09	13.2
128	SDSS J2207+2017	October 6, 2008		40	29	44	−150.75	0.17	−149.9
129	SDSS J2208+0613	July 4, 2008		15	32	50	−136.46	0.23	−135.6
130	SDSS J2213−0726	July 4, 2008		15	37	67	−392.42	0.07	−391.0

Table 2
(Continued)

ID	Object	Obs. Date (1)	Obs. Date (2)	Exp. Time (minute)	S/N (4300 Å)	S/N (5180 Å)	$V_{\rm H}$ (km s^{-1})	$\sigma(V_{\rm H})$ (km s^{-1})	$V_{\rm H}^{\rm SDSS}$ (km s^{-1})
131	SDSS J2300 + 0559	October 4, 2008		40	30	47	−244.68	0.24	−245.5
132	SDSS J2308−0855	August 22, 2008		50	32	53	−111.41	0.18	−112.4
133	SDSS J2309 + 2308[a]	July 5, 2008	July 6, 2008	50	29	49	−307.47	0.57	−308.7
134	SDSS J2334 + 1538	July 6, 2008		20	25	39	−130.09	0.29	−128.7
135	SDSS J2338 + 0902	July 5, 2008		10	27	53	−156.88	0.17	−145.6
136	SDSS J2349 + 3832[a]	August 22, 2008		30	22	37	−87.35	1.13	−84.4
137	SDSS J2357−0052[a]	October 4, 2008		15	26	47	−9.40	0.15	−14.5

Note. [a] Objects that were later observed at higher resolution and higher S/N.

open circles in Figure 3. The scatter in the $T_{\rm eff}$ comparison for these stars is 395 K, much larger than that for other stars of similar $T_{\rm eff}$ having errors smaller than 0.1 in their K magnitudes ($\sigma = 241$ K).

For the cooler stars ($T_{\rm eff} \lesssim 5500$ K), a clear offset (about 140 K) is found between the $T_{\rm eff}$ obtained from the $(V - K)_0$-based estimate and that from the SSPP, although the rms scatter is small ($\sigma = 214$ K). None of the cooler stars have K magnitude errors larger than 0.1 mag.

Estimates of $T_{\rm eff}$ based on $(g - r)_0$ color are made using the colors calculated based on ATLAS model atmosphere provided by Castelli et al.[16] For the purpose of this calculation, values of $\log g$ are assumed to be 4.0 and 2.0 for turnoff stars and giants, respectively, and the metallicity is assumed to be [Fe/H] $= -3.0$. A comparison of these $T_{\rm eff}$ estimates with those supplied by the SSPP is shown in the middle panel of Figure 3. There is no significant offset between the two estimates for turnoff stars, and the scatter is smaller (35 K) than that found for $(V - K)_0$ considered above. Although a zero-point offset is found for the giants, it is smaller (74 K) than that found for $(V - K)_0$. The reduced scatter may be a result of smaller reddening effects on the $g - r$ color than on $V - K$, or simply the better photometric precision of the measured $g - r$ colors.

For completeness, the bottom panel of Figure 3 compares the effective temperatures estimated based on the two color indices.

In order to assess the dependence of our $T_{\rm eff}$ estimates on metallicity, Figure 4 provides comparisons for three metallicity ranges. Note that we have separated this sample using the [Fe/H] values derived from the abundance analysis in the present work, as described below. No significant dependence on metallicity is seen.

Given the uncertainties in the $(V - K)_0$ based estimates, and the similarity of the $(g - r)_0$ based estimates with those from the SSPP, we simply adopt the (spectroscopic) effective temperatures determined by the SSPP for the remainder of our analysis.

4.2. Gravity, Metallicity, and Microturbulence

The $\log g$ values for turnoff stars are expected to cover the range from 3.5 (subgiant stars) to 4.5 (main-sequence stars), according to various isochrones for very metal-poor stars (Kim et al. 2002; Demarque et al. 2004). Unfortunately, for these stars, our measurements only yielded a single or a few Fe II lines, which provides little opportunity to determine $\log g$ in the traditional manner, by demanding that the same abundance be returned by analysis of the two ionization stages. Hence, the surface gravity for turnoff stars ($T_{\rm eff} > 5500$ K) is simply set to

[16] http://wwwuser.oat.ts.astro.it/castelli/colors/sloan.html

Table 3
Spectral Line Data

Species	Wavelength (Å)	$\log gf$	L.E.P. (eV)	References[a]
O I	6300.304	−9.819	0.000	1
Na I	5889.951	0.117	0.000	1
Na I	5895.924	−0.184	0.000	1
Mg I	4167.271	−0.710	4.346	2
Mg I	4571.096	−5.393	0.000	3

Notes.
[a] References – (1) Kupka et al. 1999; (2) Fischer 1975; (3) Wiese et al. 1969; (4) Aldenius et al. 2007; (5) Wiese & Martin 1980; (6) Ivans et al. 2006; (7) Lawler & Dakin 1989; (8) Blackwell et al. 1982a; (9) Blackwell et al. 1982b; (10) Pickering et al. 2001; (11) Ryabchikova et al. 1994; (12) Martin et al. 1988; (13) Booth et al. 1984; (14) O'Brian et al. 1991; (15) Schnabel et al. 2004; (16) Moity 1983; (17); Biemont et al. (1991); (18) Nitz et al. 1999; (19) Biemont & Godefroid 1980; (20) Pinnington et al. 1995; (21) Hannaford et al. 1982; (22) Gallagher 1967; (23) Lawler et al. 2001a; (24) Lawler et al. 2001b.

(This table is available in its entirety in machine-readable and Virtual Observatory (VO) forms in the online journal. A portion is shown here for guidance regarding its form and content.)

$\log g = 4.0$, and we accept that errors in its determination can be as large as 0.5 dex. We assess the impact of this assumption below.

Figure 5 shows the differences in [Fe/H] derived from Fe I and Fe II for a sample of 88 turnoff stars for which at least one Fe II line is detected. The average and standard deviation for each 0.2 dex bin of [Fe/H] are represented by an open circle and bars, respectively. No significant offset between the [Fe/H] abundances from the two species appears for [Fe/H] > -3.3. The small offset found in the lower metallicity range could be a result of a bias in the sample, arising from the fact that no Fe II line is detected for a larger fraction of these stars. Indeed, Fe II lines are detected for only 13 objects among the 24 turnoff stars with [Fe/H] < -3.3. The Fe II lines are weaker due to the generally higher gravities in objects for which the Fe II lines are not detected. Excluding this bias, the gravity adopted in our analysis for turnoff stars ($\log g = 4.0$) is well justified, based on this comparison.

The uncertainty in our $\log g$ values is estimated to be 0.5 dex, based on the standard deviation of about 0.2 dex found in Δ[Fe/H] from Fe I and Fe II (see Section 4.3 and Table 6). We note that the iron abundance measured from Fe I, which is the metallicity indicator used in this paper, as well as the abundance ratios [Mg/Fe], [Ca/Fe] and [Ba/Fe], which are important for the discussion to follow, are not very sensitive to the $\log g$ values.

We note that the $\log g$ values determined by SSPP for our turnoff stars are lower than 4.0 on average, and those for

Table 4
Steller Parameters

ID	Object	SSPP			$T_{\rm eff}$(K)	$T_{\rm eff}$(K)	Adopted Parameters		
		$T_{\rm eff}$(K)	log g	[Fe/H]	$(V-K)_0$	$(g-r)_0$	$T_{\rm eff}$(K)	log g	[Fe/H]
001	SDSS J0002 + 2928	6169	3.10	−2.81	6328	6043	6150	4.0	−3.26
002	SDSS J0008−0529	4938	2.51	−2.78	4549	4673	4950	2.0	−2.66
003	SDSS J0018−0939	4612	3.29	−2.98	4648	4628	4600	5.0	−2.65
004	SDSS J0020−0040	6453	2.69	−2.61	6055	6444	6450	4.0	−2.81
005	SDSS J0021−0050	6654	3.31	−3.09	6944	6242	6650	4.0	−3.16
006	SDSS J0023−0003	5499	2.18	−3.04	5555	5618	5500	4.0	−3.12
007	SDSS J0027 + 1404	6270	3.68	−2.88	6121	6166	6250	4.0	−3.03
008	SDSS J0027−1909	6555	3.80	−3.04	6824	6529	6550	4.0	−2.71
009	SDSS J0028−1015	6151	3.95	−2.87	6581	6152	6150	4.0	−2.81
010	SDSS J0029−1910	6499	3.75	−3.39	6750	6444	6500	4.0	−3.15
011	SDSS J0033−1859	5009	2.11	−2.83	4797	5016	5000	2.1	−2.80
012	SDSS J0041−0953	5988	2.80	−2.88	5959	5969	6000	4.0	−2.81
013	SDSS J0100 + 0049	5533	3.48	−2.95	5490	5562	5550	4.0	−3.18
014	SDSS J0111 + 1442	6330	3.70	−2.61	6323	6161	6350	4.0	−2.80
015	SDSS J0115 + 2637	5510	3.46	−2.98	5495	5535	5500	4.0	−3.32
016	SDSS J0120−1001	5801	2.77	−3.18	5702	5917	5800	4.0	−3.45
017	SDSS J0126 + 0607	6877	...	...	6842	6611	6900	4.0	−3.01
018	SDSS J0131−0908	5257	2.38	−2.79	4949	5050	5250	2.4	−2.62
019	SDSS J0140 + 2344	6103	3.37	−3.57	5890	5860	6100	4.0	−3.65
020	SDSS J0209 + 2120	6244	2.64	−2.86	5954	6190	6250	4.0	−2.89
021	SDSS J0254 + 3328	6197	3.46	−2.77	6257	6311	6200	4.0	−2.82
022	SDSS J0259 + 0057	4550	3.92	−3.62	4746	4696	4550	5.0	−3.31
023	SDSS J0308 + 0505	5938	3.05	−2.01	6136	5743	5950	4.0	−2.19
024	SDSS J0317 + 0023	5785	3.54	−3.34	5911	5913	5800	4.0	−3.39
025	SDSS J0320 + 4143	5966	4.25	−2.94	6166	6047	5950	4.0	−2.92
026	SDSS J0351 + 1026	5441	2.69	−3.09	5645	5723	5450	3.6	−3.18
027	SDSS J0414 + 0552	6514	3.69	−2.84	7020	6534	6500	4.0	−2.32
028	SDSS J0416 + 0713	5956	3.20	−2.19	5464	5264	5950	4.0	−2.59
029	SDSS J0629 + 8303	5539	2.51	−3.00	5542	5439	5550	4.0	−2.82
030	SDSS J0630 + 2552	6100	3.77	−3.15	7493	6185	6100	4.0	−3.05
031	SDSS J0711 + 6702	5338	2.32	−2.57	5237	5235	5350	3.0	−2.91
032	SDSS J0723 + 3637	5135	2.98	−3.35	4992	5113	5150	2.2	−3.32
033	SDSS J0727 + 1609	6613	4.02	−2.82	6124	6276	6600	4.0	−2.92
034	SDSS J0741 + 6708	5201	2.40	−2.94	5006	5116	5200	2.5	−2.87
035	SDSS J0746 + 2831	6111	4.15	−2.77	6313	6038	6100	4.0	−2.75
036	SDSS J0748 + 1758	6091	3.36	−2.81	6311	6176	6100	4.0	−2.60
037	SDSS J0749 + 1801	5098	2.85	−2.80	4978	5037	5100	1.8	−2.64
038	SDSS J0804 + 5153	5948	3.14	−2.74	5693	5873	5950	4.0	−3.01
039	SDSS J0809 + 0907	6155	3.16	−3.37	6285	6214	6150	4.0	−3.38
040	SDSS J0814 + 3337	6454	3.34	−3.14	6590	6469	6450	4.0	−3.28
041	SDSS J0817 + 2641	6053	3.40	−3.17	6277	6109	6050	4.0	−2.85
042	SDSS J0819 + 3119	6327	4.07	−2.75	6455	6385	6350	4.0	−2.88
043	SDSS J0821 + 1819	6269	3.80	−3.25	6187	6242	6250	4.0	−3.70
044	SDSS J0825 + 0403	6414	3.35	−3.42	5653	6444	6400	4.0	−3.60
045	SDSS J0827 + 1052	6409	3.88	−3.23	6230	6365	6400	4.0	−3.17
046	SDSS J0840 + 5405	6152	3.45	−2.92	5766	6286	6150	4.0	−3.25
047	SDSS J0847 + 0121	6271	3.83	−3.01	6199	6419	6250	4.0	−3.20
048	SDSS J0851 + 1018	6486	3.80	−2.94	6438	6281	6500	4.0	−2.89
049	SDSS J0858 + 3541	5192	1.99	−2.76	5075	5001	5200	2.5	−2.53
050	SDSS J0859 + 0402	5416	3.70	−3.04	5188	5225	5400	3.1	−3.05
051	SDSS J0907 + 0246	5985	2.89	−3.39	6293	6066	6000	4.0	−3.30
052	SDSS J0912 + 0216	6127	2.55	−2.85	6275	5952	6150	4.0	−2.68
053	SDSS J0932 + 0241	6220	3.32	−2.89	5910	6405	6200	4.0	−3.14
054	SDSS J1004 + 3442	6114	3.14	−3.05	6035	6076	6100	4.0	−3.09
055	SDSS J1033 + 4001	6582	3.83	−2.90	6323	6464	6600	4.0	−3.06
056	SDSS J1036 + 1212	5854	3.13	−3.45	5787	5917	5850	4.0	−3.47
057	SDSS J1106 + 0343	6281	4.10	−2.89	7010	6185	6300	4.0	−2.88
058	SDSS J1108 + 1747	6051	3.35	−2.84	6201	6024	6050	4.0	−3.17
059	SDSS J1120 + 3027	5750	4.32	−3.02	5810	5671	5750	4.0	−3.14
060	SDSS J1128 + 3841	6570	3.68	−3.26	6621	6565	6550	4.0	−2.82
061	SDSS J1147 + 1510	6499	3.70	−2.98	6876	6459	6500	4.0	−2.96
062	SDSS J1159 + 5425	5721	3.09	−3.25	5886	5702	5700	4.0	−3.26
063	SDSS J1213 + 4450	6637	4.34	−3.11	6230	6719	6650	4.0	−3.20
064	SDSS J1230 + 0005	6160	2.90	−3.56	6153	6271	6150	4.0	−3.34
065	SDSS J1233 + 3407	6325	3.61	−2.64	6173	6133	6300	4.0	−2.87

Table 4
(Continued)

ID	Object	SSPP			$T_{\rm eff}$(K)	$T_{\rm eff}$(K)	Adopted Parameters		
		$T_{\rm eff}$(K)	log g	[Fe/H]	$(V-K)_0$	$(g-r)_0$	$T_{\rm eff}$(K)	log g	[Fe/H]
066	SDSS J1241−0837	5138	2.47	−2.72	4901	4956	5150	2.5	−2.73
067	SDSS J1242−0336	5130	2.63	−2.86	4961	5087	5150	2.5	−2.77
068	SDSS J1245−0738	6108	...	...	6393	6142	6100	4.0	−3.17
069	SDSS J1300 + 2632	6464	3.30	−3.26	6510	6385	6450	4.0	−3.53
070	SDSS J1303 + 2515	6141	3.74	−2.71	6323	6147	6150	4.0	−2.85
071	SDSS J1304 + 3239	6054	3.62	−2.96	6534	6331	6050	4.0	−2.90
072	SDSS J1312 + 2450	6251	3.64	−2.75	6069	6199	6250	4.0	−2.72
073	SDSS J1316 + 1747	4976	2.19	−2.23	4579	4662	5000	2.1	−2.10
074	SDSS J1334 + 0022	5664	3.21	−3.03	5555	5626	5650	4.0	−3.03
075	SDSS J1338 + 1204	6281	4.07	−2.89	6445	6218	6300	4.0	−2.86
076	SDSS J1349−0229	6189	...	...	5725	6081	6200	4.0	−3.24
077	SDSS J1400 + 0753	6274	3.74	−2.87	5882	6276	6250	4.0	−2.98
078	SDSS J1408 + 6239	6284	4.41	−2.88	6420	6340	6300	4.0	−2.97
079	SDSS J1410 + 5350	6102	3.40	−3.15	6402	6199	6100	4.0	−3.42
080	SDSS J1412 + 5609	6608	3.98	−3.24	6420	6867	6600	4.0	−3.19
081	SDSS J1422 + 0031	5190	2.45	−3.17	4865	5850	5200	2.2	−3.03
082	SDSS J1424 + 5615	6339	3.95	−3.04	5971	6266	6350	4.0	−2.97
083	SDSS J1425 + 1137	6272	3.99	−2.98	6292	6370	6300	4.0	−3.08
084	SDSS J1425 + 5742	6474	3.90	−3.15	6345	6580	6450	4.0	−3.29
085	SDSS J1434 + 1036	6396	3.43	−3.22	5397	6326	6400	4.0	−3.21
086	SDSS J1436 + 0918	6521	3.61	−3.26	6886	6385	6500	4.0	−3.49
087	SDSS J1436 + 0301	6175	3.04	−3.22	6047	6176	6150	4.0	−3.60
088	SDSS J1437 + 5231	6292	4.02	−2.99	6480	6335	6300	4.0	−2.90
089	SDSS J1437 + 5837	6460	3.47	−2.77	6464	6335	6450	4.0	−3.02
090	SDSS J1446 + 1249	6346	3.61	−3.01	6024	6355	6350	4.0	−2.99
091	SDSS J1502 + 3113	6347	3.95	−2.77	6404	6439	6350	4.0	−2.86
092	SDSS J1504 + 4623	6069	3.65	−3.27	6206	6218	6050	4.0	−3.31
093	SDSS J1515 + 4503	6312	3.76	−3.06	6508	6128	6300	4.0	−3.34
094	SDSS J1516 + 4333	6517	3.49	−2.78	6570	6596	6500	4.0	−2.91
095	SDSS J1521 + 3437	6203	3.81	−2.86	6507	6109	6200	4.0	−2.79
096	SDSS J1522 + 3055	6008	2.77	−3.46	5873	5908	6000	4.0	−3.59
097	SDSS J1523 + 4942	5846	3.41	−2.92	5779	5791	5850	4.0	−3.06
098	SDSS J1528 + 4915	6441	3.34	−3.06	6483	6555	6450	4.0	−2.99
099	SDSS J1551 + 2521	5854	3.85	−3.05	5899	5961	5850	4.0	−3.07
100	SDSS J1553 + 2511	5861	2.31	−2.86	5687	5679	5850	4.0	−3.30
101	SDSS J1603 + 2917	6007	3.97	−3.13	6432	6104	6000	4.0	−3.36
102	SDSS J1612 + 0421	5364	2.58	−2.88	5450	5371	5350	3.3	−2.86
103	SDSS J1613 + 5309	5333	2.51	−2.80	5184	5307	5350	2.1	−3.33
104	SDSS J1623 + 3913	6369	3.81	−2.79	6580	6214	6350	4.0	−3.19
105	SDSS J1626 + 1458	6385	...	...	5907	6390	6400	4.0	−2.99
106	SDSS J1633 + 3907	6288	3.53	−2.95	5699	6171	6300	4.0	−2.88
107	SDSS J1640 + 3709	6435	3.41	−3.29	6319	6350	6450	4.0	−3.39
108	SDSS J1646 + 2824	6109	2.78	−2.71	6532	5996	6100	4.0	−3.05
109	SDSS J1650 + 2242	6577	3.90	−2.96	6691	6340	6600	4.0	−2.56
110	SDSS J1659 + 3515	6073	3.17	−2.93	5992	6223	6050	4.0	−3.24
111	SDSS J1703 + 2836	5119	4.37	−3.48	5057	5109	5100	4.8	−3.21
112	SDSS J1728 + 0657	6333	3.62	−3.08	6832	6316	6350	4.0	−2.85
113	SDSS J1734 + 4316	5196	1.33	−3.01	5237	5095	5200	2.7	−2.51
114	SDSS J1735 + 4446	5266	2.95	−3.14	4868	5100	5250	2.0	−3.29
115	SDSS J1736 + 4420	5475	2.96	−2.83	5173	5227	5450	3.0	−2.93
116	SDSS J1746 + 2455	5358	2.47	−2.85	5030	5164	5350	2.6	−3.17
117	SDSS J1830 + 4141	6571	3.87	−3.08	6568	6637	6550	4.0	−3.01
118	SDSS J1834 + 2023	6528	3.18	−2.72	6397	6632	6550	4.0	−1.98
119	SDSS J1836 + 6317	5341	1.55	−2.73	5575	5037	5350	3.0	−2.85
120	SDSS J2005−1045	6614	3.90	−3.46	6332	6380	6600	4.0	−3.34
121	SDSS J2052 + 0109	6067	4.30	−2.68	6183	6009	6050	4.0	−2.80
122	SDSS J2104−0104	5275	2.74	−2.99	5379	5279	5250	2.0	−3.43
123	SDSS J2111 + 0109	6270	3.18	−2.63	6235	6271	6250	4.0	−2.75
124	SDSS J2118−0640	6651	3.92	−2.78	6603	6375	6650	4.0	−2.91
125	SDSS J2123−0820	6344	3.54	−2.71	6100	5974	6350	4.0	−2.88
126	SDSS J2128−0756	6148	3.41	−2.84	5903	6214	6150	4.0	−2.76
127	SDSS J2206−0925	5084	2.62	−3.08	4911	5031	5100	2.1	−3.17
128	SDSS J2207 + 2017	6192	3.49	−3.05	6491	6488	6200	4.0	−2.42
129	SDSS J2208 + 0613	6432	3.56	−2.78	6408	6296	6450	4.0	−2.85
130	SDSS J2213−0726	5135	2.35	−2.56	4724	4867	5150	1.8	−2.55

Table 4
(Continued)

ID	Object	SSPP				$T_{\rm eff}$(K)	$T_{\rm eff}$(K)	Adopted Parameters		
		$T_{\rm eff}$(K)	log g	[Fe/H]		$(V-K)_0$	$(g-r)_0$	$T_{\rm eff}$(K)	log g	[Fe/H]
131	SDSS J2300 + 0559	6505	3.94	−2.94	6289	6326	6450	4.0	−2.94	
132	SDSS J2308−0855	6086	3.55	−2.90	6891	6000	6100	4.0	−2.74	
133	SDSS J2309 + 2308	6337	3.70	−3.00	6013	5904	6350	4.0	−3.09	
134	SDSS J2334 + 1538	6558	4.33	−2.91	6510	6405	6550	4.0	−2.91	
135	SDSS J2338 + 0902	4889	2.33	−3.23	4570	4602	4900	1.9	−3.12	
136	SDSS J2349 + 3832	6233	3.16	−3.35	5990	6550	6250	4.0	−3.20	
137	SDSS J2357−0052	5209	3.98	−3.41	5105	5055	5200	4.8	−3.20	

47 stars are lower than 3.5. We suspect that the uncertainty in gravity determination by the SSPP for EMP stars is still larger than the errors estimated for the entire SSPP sample (see Section 2.1), and further calibration for the lowest metallicity range is required.

For giants, where greater numbers of Fe II lines are detectable, the log g values are determined by seeking agreement between the iron abundances derived from the Fe I and Fe II lines, within measurement errors (Table 4). Note that our sample includes four cool stars ($T_{\rm eff} \leqslant 5200$ K) that exhibit very weak features of ionized species, including Fe II, compared to red giants of similar temperatures, indicating that they are on the main sequence. Two of them (SDSS 1703+2836 and SDSS 2357–0052) have already been studied by Aoki et al. (2010). The surface gravities of these stars are estimated by reading off the value from an isochrone appropriate for low-mass metal-poor stars with ages of 12 Gyr (Kim et al. 2002), as was also done by Aoki et al. (2010). We adopt log $g = 4.8$ for the two stars studied by Aoki et al. (2010), and 5.0 for the other two cooler objects. The high surface gravity for these stars explains the strong features of the Mg I b lines, due to the broader wings, as well as the detectable CH G-band, without assuming exceptional overabundances of C and Mg.

The microturbulent velocity, $v_{\rm micro}$, for turnoff stars is fixed to 1.5 km s^{-1}, which is a typical value found by previous studies (e.g., Cohen et al. 2004). Since the abundance measurements for most elements in turnoff stars are based on weak lines, the result is insensitive to the adopted microturbulent velocity. The values for giants are determined from the analysis of Fe I lines, by forcing the iron abundances from individual lines to exhibit no dependence on the measured equivalent widths. The $v_{\rm micro}$ of cool main-sequence stars is assumed to be zero, which best explains the relation between the equivalent widths of Fe I lines and the abundances from individual lines. There remains a weak trend in the relation, which can be resolved by assuming negative values for $v_{\rm micro}$. This suggests that the line broadening from the Unsöld approximation should not be enhanced, as discussed by Aoki et al. (2010).

The metallicity of the model atmospheres ([M/H] = [Fe/H]) is fixed to −3.0. The temperature/density structure of photospheres, and the chemical abundances derived using model atmospheres, is not very sensitive to the assumed metallicity in such very/extremely metal-poor stars. Exceptions are found for the three stars for which [Fe/H] > -2.5 was derived; in such cases we iterated the analysis to obtain consistent [Fe/H] values.

Figure 1 shows the [Fe/H] abundances determined by the analysis of high-resolution spectra compared with those supplied by the SSPP for SDSS medium-resolution spectra. The upper panel shows the comparison for the estimates from SDSS spectra which were available when target selection for the Subaru observations was carried out in 2008. This comparison indicates that very/extremely metal-poor stars are efficiently selected from the SDSS measurements. Among the targets for which [Fe/H] is estimated to be lower than −2.7 from the SSPP estimate (most of objects in our sample, with few exceptions), only 10 stars have high-resolution determinations [Fe/H] > -2.7. This demonstrates a clear advantage of using the results of the SDSS survey for picking EMP targets, relative to previous surveys based on low-resolution objective-prism spectra.

On the other hand, the correlation between the two measurements of [Fe/H] is weak, as seen in the upper panel of Figure 1. In particular, stars for which the iron abundance is estimated to be $-3.0 <$ [Fe/H] < -2.7 exhibit very large scatter. Since the number of objects that have high [Fe/H] ([Fe/H] > -2.5; measured from high-resolution spectra) is small, the large scatter is due to the existence of many EMP ([Fe/H] < -3.0) stars among them. Moreover, almost all stars for which [Fe/H] < -3 as derived from the SDSS spectra exhibit lower [Fe/H] as obtained from the high-resolution spectra. This comparison indicates that the criterion in the sample selection for the [Fe/H] values from SDSS (based on an earlier version of SSPP) provides a homogeneous sample for lower metallicity ([Fe/H] $\lesssim -3$), while the selection could be incomplete for stars of higher metallicity.

The lower panel of Figure 1 shows a comparison of [Fe/H] abundances derived by our analysis of high-resolution spectra with the SDSS estimates supplied by the latest version of SSPP. In contrast to the upper panel, there is no clear offset between the two estimates. However, the scatter is still larger than preferred for detailed inference of, e.g., the nature of the metallicity distribution function (MDF) at very/extremely low metallicity. We also note that, in particular for metallicities as low as those considered in our present analysis, the effects of interstellar Ca II on metallicities calculated from medium-resolution spectra can be large, in particular for warmer stars, which rely almost entirely on the strength of the Ca II K line for their metallicity estimation. Thus, we are reminded once again that high-resolution spectroscopy is required to obtain accurate metallicity estimates for individual EMP stars.

The [Fe/H] values we estimate for the four cool main-sequence stars from our high-resolution spectra are lower than those from the SSPP, by ∼0.3 dex. The gravity estimates for these stars are also significantly higher than reported by the SSPP for the medium-resolution spectra, which may also contribute some to the offset in [Fe/H]. It should be kept in mind that, due to their low luminosities, cool dwarfs infrequently enter into samples of VMP/EMP stars selected from magnitude limited samples. Nevertheless, future adjustments to the SSPP may be able to better handle such stars.

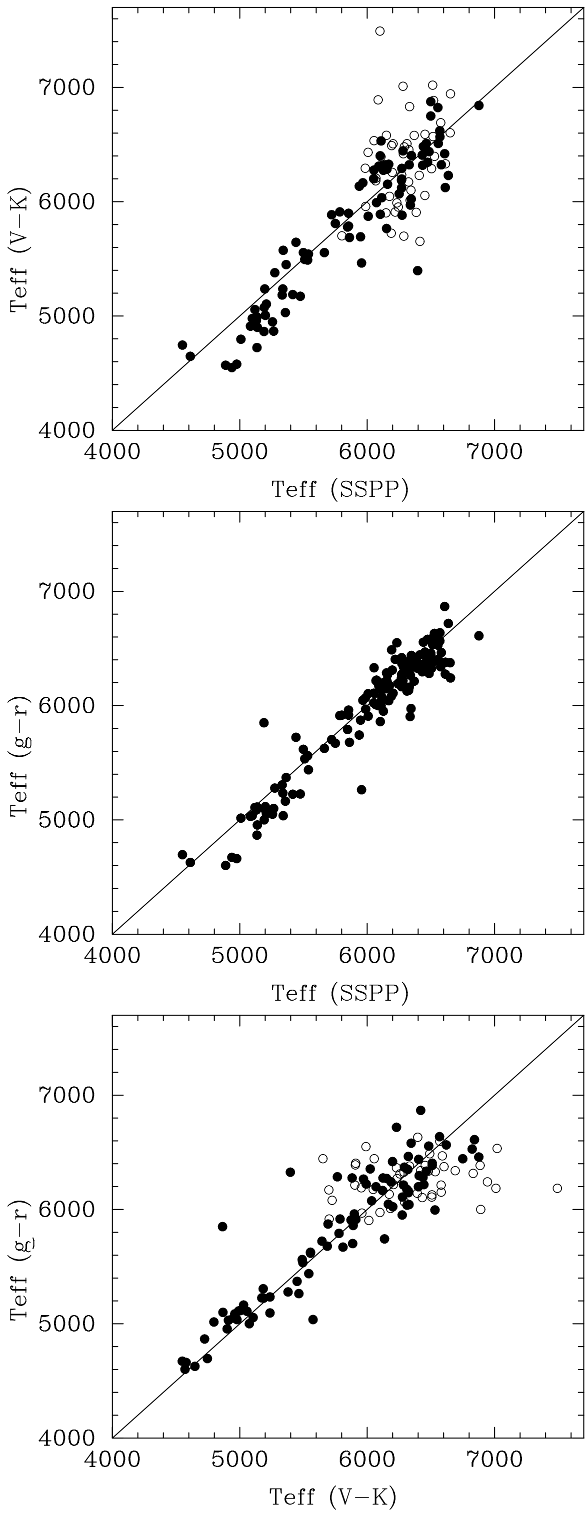

Figure 3. Comparison of T_{eff} estimated by the (recent) SSPP and that from $(V - K)_0$ (top panel) and from $(g - r)_0$ (middle panel). The bottom panel shows the comparison of T_{eff} between the two color indices. The open circles indicate objects with large errors in their K-band photometry.

4.3. Abundance Measurements

Standard LTE abundance analyses for measured equivalent widths have been made for other elements. The derived abundances are presented in Table 5. The errors given in the table include random errors and those due to uncertainties of atmospheric parameters. The random errors in the measurements are

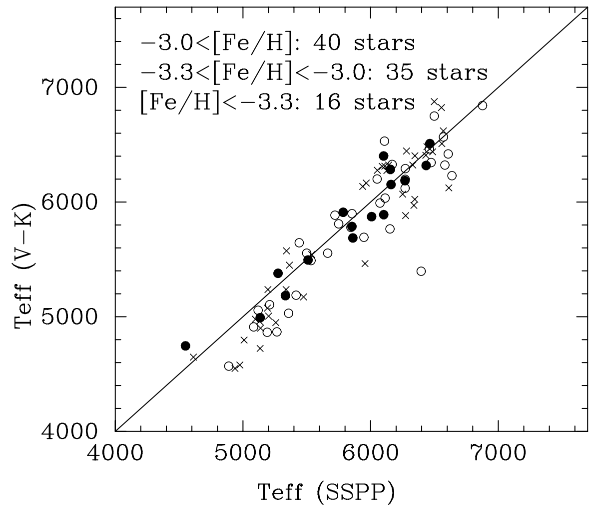

Figure 4. Comparison of T_{eff} , estimated by the (recent) SSPP, and those from $(V - K)_0$. The sample is separated into three metallicity ranges ([Fe/H] < -3.3: filled circles, $-3.3 <$ [Fe/H] < -3.0: open circles, and $-3.0 <$ [Fe/H]: crosses).

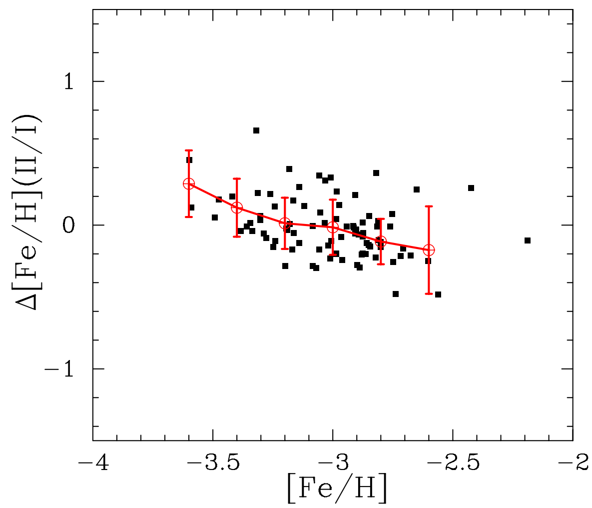

Figure 5. Difference of [Fe/H] derived from Fe I and Fe II for main-sequence turnoff stars (filled squares). The average and standard deviation for each 0.2 dex bin of [Fe/H] are represented by open circles and bars, respectively. The standard deviations are about 0.20 dex, which is as small as the random errors in the abundance measurements. The lowest metallicity range likely suffers from a bias, in that no Fe II line is detected for a larger fraction of stars than the less metal-poor stars. (See the text for details.)

(A color version of this figure is available in the online journal.)

estimated to be $\sigma N^{-1/2}$, where σ is the standard deviation of derived abundances from individual lines, and N is the number of lines used. Since the N for most elements other than Fe is small, the σ of Fe I ($\sigma_{\mathrm{Fe\,I}}$) is adopted in the estimates for them (i.e., error is $\sigma_{\mathrm{Fe\,I}} N^{-1/2}$). The errors due to the uncertainty of the atmospheric parameters are estimated for a turnoff star and a giant (Table 6), for $\delta T_{\mathrm{eff}} = 150$ K, $\delta \log g = 0.5$, and $\delta v_{\mathrm{micro}} = 0.5$ km s^{-1}). These errors are added in quadrature to the random errors to derive the total errors given in Table 5.

4.4. Carbon Abundances

Carbon abundances are determined for 28 stars in our sample, based on the CH G-band (the Q branches of CH A–X system at $\sim$4320 Å), as well as the C_2 Swan 0–0 band at 5165 Å. Examples of the spectra of the CH band are shown in Figure 6.

Table 5
Chemical Abundances Results

	Fe (Fe I)[a]	Fe (Fe II)	Na	Mg	Ca	Ti	Sr	Ba	C
001				SDSS J0002+2928					
$\log\epsilon$	4.24	4.59	3.97	4.70	2.87	2.49	−0.12	0.75	7.80
[X/Fe]	−3.26	0.35	1.00	0.36	−0.20	0.80	0.27	1.84	2.63
σ_{tot}	0.21	0.30	0.24	0.16	0.21	0.27	0.29	0.27	0.22
N	11	2	1	2	1	4	1	2	...
002				SDSS J0008−0529					
$\log\epsilon$	4.84	4.86	3.79	5.18	3.77	2.61	0.24	0.35	...
[X/Fe]	−2.66	0.02	0.21	0.24	0.09	0.32	0.03	0.83	...
σ_{tot}	0.34	0.34	0.24	0.16	0.18	0.30	0.35	0.39	...
N	64	6	2	5	9	17	1	2	...

Note. [a] [Fe/H] value is given for [X/Fe].

(This table is available in its entirety in machine-readable and Virtual Observatory (VO) forms in the online journal. A portion is shown here for guidance regarding its form and content.)

Table 6
Abundance Changes by Changing Atmospheric Parameters

SPECIES	Giant					Turnoff				
	$\delta T_{\rm eff}$	$\delta\log g$	δ[Fe/H]	$\delta v_{\rm micro}$	r.s.s.	$\delta T_{\rm eff}$	$\delta\log g$	δ[Fe/H]	$\delta v_{\rm micro}$	r.s.s
Fe (Fe I)	0.19	−0.10	0.00	−0.26	0.33	0.13	−0.04	0.01	0.14	0.20
Na	−0.03	0.03	0.00	−0.12	0.13	−0.03	0.03	0.00	−0.12	0.13
Mg	−0.01	−0.10	−0.01	0.03	0.10	−0.02	−0.05	0.00	−0.02	0.06
Ca	0.05	−0.14	0.00	0.03	0.15	−0.02	−0.01	0.00	−0.04	0.04
Ti (Ti II)	−0.11	0.24	0.00	0.13	0.30	−0.07	0.21	−0.01	−0.12	0.25
Fe (Fe II)	−0.16	0.25	0.00	0.13	0.32	−0.11	0.21	−0.01	−0.12	0.26
Sr	−0.05	0.19	0.00	−0.04	0.20	−0.05	0.19	0.00	−0.04	0.20
Ba	−0.07	0.25	0.00	0.22	0.34	−0.04	0.20	0.00	−0.11	0.23

The molecular data are the same as those used in Aoki et al. (2007).

The CH G-band is detected for 14 stars among the 25 giants, and for all four of the cool main-sequence stars. Nine giants are carbon-enhanced ([C/Fe] $> +0.7$). The C_2 band is used to determine the carbon abundances of four stars, because the CH G-band in these objects is almost saturated. The detection limit of the CH G-band in a red giant with $T_{\rm eff} < 5500$K is approximately [C/H] ~ -2.5 for spectra of snapshot quality (S/N $\sim$ 30). Hence, stars for which the CH G-band feature is not detected are unlikely to be CEMP stars. The fraction of CEMP stars in our sample is $9/25 \sim 36\%$, which is in agreement with the estimate by Carollo et al. (2012) for [Fe/H] ~ -3, i.e., at the limit of their sample.

None of the four cool main-sequence stars in our sample are carbon enhanced. The CH G-band is detected for such objects because of their low temperatures and the high pressure of their atmospheres. Among the four stars, the lowest carbon abundance ratio is found for SDSS J0018-0939 ([C/Fe] $= -0.7$). Although the CH G-band of this star is weak and the measurement is uncertain, a conservative upper limit is [C/Fe] < -0.3, which is already lower than the carbon abundances found in other cool main-sequence stars. A weak CH G-band could alternatively be explained by assuming a lower gravity. However, the weak features of ionized species such as Fe II cannot be accounted for if this object is assumed to be a red giant ($\log g < 3$). Thus, the underabundance of carbon in this star is a robust result, although a higher quality spectrum is required to derive an accurate estimate of its abundance.

In contrast to the giants, the CH G-band is detected for only 10 stars among the 108 turnoff stars. All of these objects are highly carbon enhanced ([C/Fe] $\gtrsim +2$). The detection limit of the CH G-band for a turnoff star with $T_{\rm eff} \sim 6000$ K is [C/H] ~ -1.5 ([C/Fe] $\sim +1.5$ for [Fe/H] ~ -3), indicating that the CH G-band is not measurable even for the mildly carbon-enhanced ($+0.7 <$ [C/Fe] $< +1.5$) stars in our sample. Hence, the fraction of CEMP objects for the turnoff stars ($10/108 \sim 9\%$) should be regarded as a lower limit.

4.5. Analysis of the Comparison Star G 64–12

In order to examine the reliability of the abundances determined from our snapshot spectra, we obtained a spectrum of the well-studied EMP turnoff star G 64–12, using the same instrumental setup and integrating to a similar S/N ratio as for the bulk of our sample, employing a short (five minute) exposure time. The chemical composition of this object was reported on by Aoki et al. (2006), using a high-resolution, high-S/N spectrum. The abundance analysis for this object was conducted adopting the same model atmosphere used in Aoki et al. (2006), that is, the ATLAS model including convective overshooting (Kurucz 1993) for $T_{\rm eff} = 6380$ K, $\log g = 4.4$ and [Fe/H] $= -3.2$. The results are compared in Table 7. The [Fe/H] and [X/Fe] values are calculated adopting the solar abundances of Asplund et al. (2009) for both cases. The agreement is fairly good for most species: the differences of the two measurements ($\log\epsilon$ values) are within 0.12 dex, which are as small as the random errors in the present analyses. An exception is the Sr abundance, which is determined from the Sr II resonance lines in the blue range, where the data quality is relatively low. Another exception is Na, for which only a preliminary result was provided in Aoki et al. (2006). The Na abundance was determined from the same

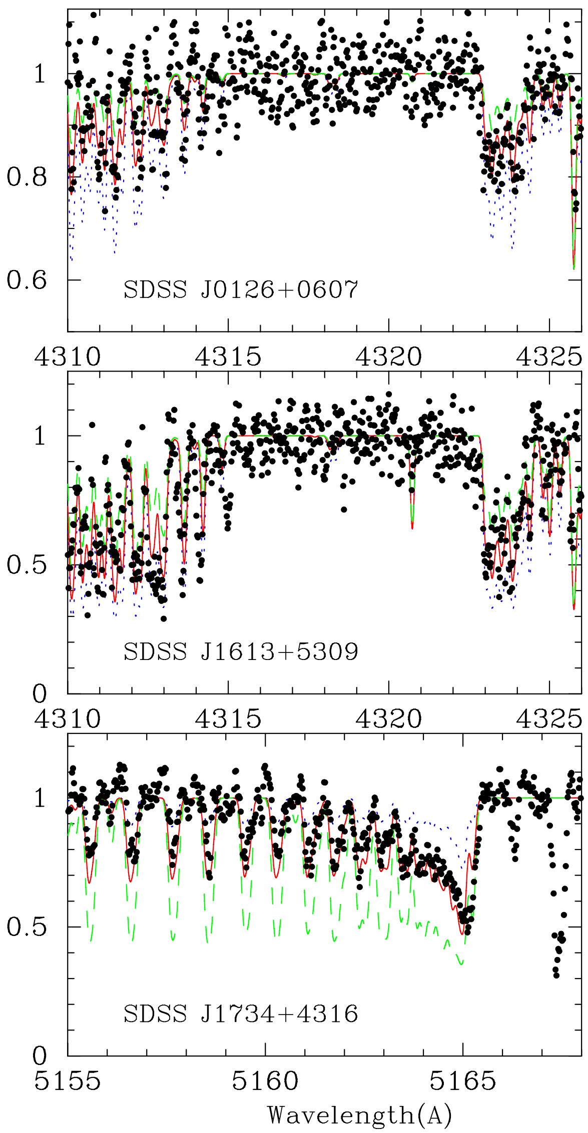

Figure 6. Spectra of the CH *G*-band/4323 Å band and the C_2 Swan band at 5165 Å, for the stars labeled in each panel (filled circles). The three synthetic spectra are calculated by changing [C/Fe] by 0.3 dex (dashed and dotted lines) around the adopted values (solid line).

(A color version of this figure is available in the online journal.)

Table 7
Chemical Abundances of G 64–12

Element	Species	This Work		Aoki et al. (2006)	
		log ϵ	[X/Fe]	log ϵ	[X/Fe]
Fe	Fe I	4.36	−3.14	4.25	−3.25
Fe	Fe II	4.24	−3.26	4.38	−3.12
Na	Na I	2.82	−0.28	2.74[a]	. . .
Mg	Mg I	4.79	0.33	4.80	0.45
Ca	Ca I	3.50	0.30	3.62	0.53
Ti	Ti II	2.27	0.46	2.20	0.50
Sr	Sr II	−0.35	−0.08	−0.10	0.28

Note. [a] Value adopted from Aoki et al. (2009).

spectrum to be $\log \epsilon(\mathrm{Na}) = 2.74$ by Aoki et al. (2009), adopting slightly different atmospheric parameters (Table 7), which agrees well with the Na abundance measured by the present work ($\log \epsilon(\mathrm{Na}) = 2.82$).

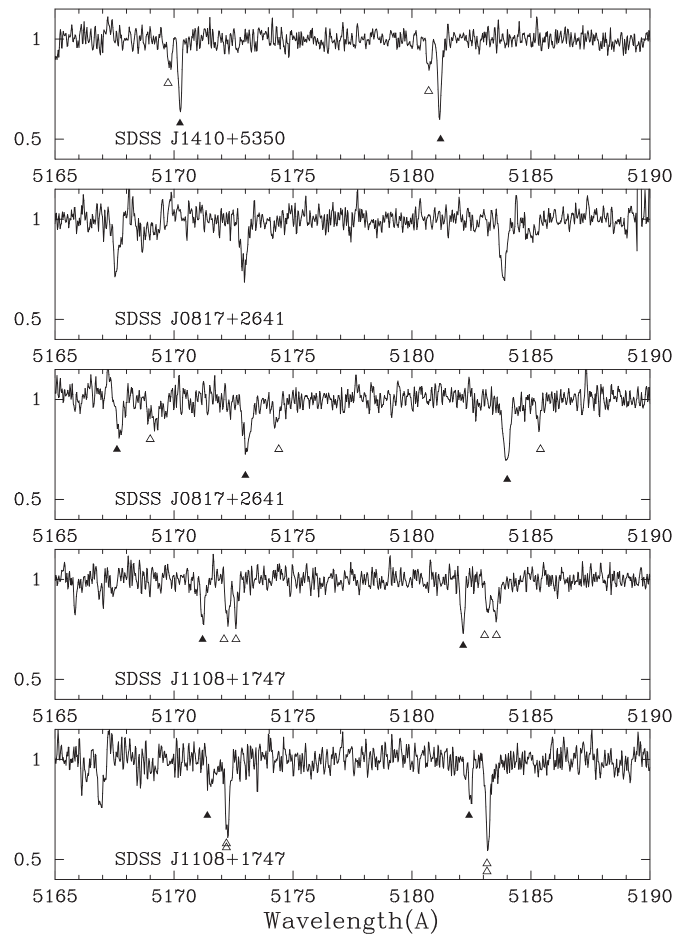

Figure 7. Spectra around the Mg b lines of double-lined and triple-lined spectroscopic binaries: SDSS J1410+5350 (the top panel), SDSS J0817+2641 (second and third panels), and SDSS J1108+1747 (the lower two panels). The filled triangles indicate the primary Mg I b lines for each star, while the open triangles show the secondary ones.

4.6. Double-lined Spectroscopic Binaries

Three stars in our sample clearly exhibit two (or three, in the case of one star) sets of absorption features with distinct Doppler shifts, suggesting these objects to be double-lined spectroscopic binaries or multiple systems. The region of the spectra around the Mg b lines of these objects is shown in Figure 7.

SDSS J0817+2641 was already studied by Aoki et al. (2008). The spectrum obtained in their study (on 2007 February 9) is shown in the second panel of Figure 7. The second component of the absorption features is not obvious in their spectrum, while it is clearly seen in our new spectrum shown in the third panel. Aoki et al. (2008) reported a discrepancy in the radial velocities measured from the SDSS medium-resolution spectrum and their Subaru high-resolution data. The discrepancy is most likely a result of the large Doppler shifts of both components, or possibly due to the uncertainty of the measurements from the medium-resolution spectrum, which was incapable of resolving the two components. This also suggests that, given the overall excellent quality of the SDSS stellar velocity determinations (especially for the brighter stars one naturally targets for high-resolution spectroscopic follow-up), as described in Section 3.2, that obtaining even a single-epoch snapshot quality high-resolution spectrum is an efficient way to identify at least high-amplitude binary variations in a sample of stars.

The spectrum of SDSS J1108+1747, obtained on 2008 March 7 (fourth panel of Figure 7) exhibits triple spectral features, indicating that this system consists of at least three stars of similar luminosity. A significant change of the spectral features is found in its March 9 spectrum (fifth panel), in which only two components appear. The correspondence between the features of the two spectra is still unclear because of the limited quality of our spectra. This is, to our knowledge, the most metal-deficient multiple ($n \geqslant 3$) system yet discovered ([Fe/H] ~ -3).

In order to accurately measure the chemical compositions of these objects, we need to determine the contribution of each component to the continuum light. This is only possible by determining the mass ratios from long-term radial velocity monitoring. However, the ratios of the apparent strengths of the Mg b lines (depths of the absorption lines) are at most three or four, suggesting that the components have comparable luminosities. The objects have $T_{\rm eff}$ around 6000 K. Hence, the spectral features can be modeled by adding the spectra of two or three main-sequence stars that have slightly different mass (mass ratios of 1.2 or smaller; see Goldberg et al. 2002), which have similar strengths of the (partially saturated) Mg b lines. For a rough estimate of the contribution of each component to the continuum light, we assume that the contribution is in proportion to the depth of the Mg b absorption lines. The primary components of the Mg b lines identified by the present work are indicated by the filled triangles in Figure 7. The contributions of the primary components estimated by this method are 75%, 80%, and 40% in SDSS J1410+5350, SDSS J0817+2641, and SDSS J1108+1747, respectively. The equivalent widths measured for the primary components by Gaussian fitting are divided by these factors for carrying out the abundance analyses.

The abundance analyses for the primary components of these objects are made as for other single-lined stars. We adopt the $T_{\rm eff}$ determined by SSPP with no modification; the $T_{\rm eff}$'s estimated from colors agree with the SSPP results. The colors of the (integrated) system should be similar to the colors of the primary component—if the primary is distinctively warmer than the other components, it should dominate the system luminosity, while the primary should have similar $T_{\rm eff}$ to the other components if it does not dominate the system luminosity.

5. DISCUSSION

5.1. Carbon-enhanced Metal-poor Stars

Previous studies of CEMP stars have clearly demonstrated that they are separable into at least two primary classes: CEMP stars exhibiting large enhancements of s-process elements (CEMP-s), and those with no excess of neutron-capture elements (CEMP-no) (Beers & Christlieb 2005). Note that recent studies of CEMP-s stars split this class even more granularly (e.g., Bisterzo et al. 2011). The fraction of CEMP-no stars among all CEMP stars is $\sim$20%, and increases with decreasing stellar metallicity (Aoki et al. 2007; Hollek et al. 2011). The distribution of the [C/H] ratios also appears to be different between the two classes—most of the CEMP-s stars exhibit quite high values ([C/H] > -1), while the CEMP-no class exhibits a wide distribution of values (Aoki et al. 2007).

Among the nine CEMP red giants in our sample, only two possess large excesses of Ba ([Ba/Fe] $> +1$: SDSS J1836+6317 and SDSS J1734+4316). One exhibits a moderate excess of Ba ([Ba/Fe] $= +0.8$: SDSS J0711+6702). Four stars have solar or lower Ba abundance ratios ([Ba/Fe] $\lesssim 0$), hence are classified as CEMP-no stars. Although Ba is not measured for the other two CEMP red giants, they could also be CEMP-no, given the detection limit of Ba in red giants ([Ba/Fe] ~ -0.5 at [Fe/H] ~ -3). Hence, six objects among the nine CEMP giants in our sample are CEMP-no stars. This result suggests that a high fraction of CEMP-no stars exists in this metallicity range ($-3.4 <$ [Fe/H] < -2.5).

Possible progenitors for the CEMP-no class include massive, rapidly rotating, mega metal-poor ([Fe/H] < -6.0) stars, which models suggest have greatly enhanced abundances of CNO due to distinctive internal burning and mixing episodes, followed by strong mass loss (Hirschi et al. 2006; Meynet et al. 2006, 2010a, 2010b). Another suggested mechanism for the production of the material incorporated into CEMP-no stars is pollution of the interstellar medium by so-called faint supernovae associated with the first generations of stars, which experience extensive mixing and fall back during their explosions (Umeda & Nomoto 2003, 2005; Tominaga et al. 2007). This model well reproduces the observed abundance pattern of the CEMP-no star BD+44°493, the ninth-magnitude [Fe/H] $= -3.7$ star (with [C/Fe] $= +1.3$, [N/Fe] $= +0.3$, [O/Fe] $= +1.6$) discussed by Ito et al. (2009). The recently reported high redshift ($z = 2.3$), extremely metal-poor damped Lyα (DLA) system by Cooke et al. (2011 : [Fe/H] ~ -3.0) exhibits enhanced carbonicity ([C/Fe] $= +1.5$) and other elemental abundance signatures that Kobayashi et al. (2011) also associate with production by faint supernovae. In addition, a fraction of CEMP-no stars might belong to binary systems and have been formed by mass transfer from asymptotic giant branch (AGB) stars that yielded no s-process elements but enriched carbon (e.g., Suda et al. 2004).

Eight of the 10 CEMP turnoff stars exhibit large enhancements of Ba. Although the metallicities of these stars are similar to those of the CEMP giants, the fraction of CEMP-s stars is apparently higher among the turnoff stars than for the red giants. The carbon overabundances of all the CEMP turnoff stars are much larger than the average overabundances of the CEMP giants, presumably because the detection limit of the CH *G*-band is higher for these warmer stars. As shown by previous studies of CEMP stars (e.g., Aoki et al. 2007), the [C/H] distributions are quite different between the two classes of CEMP stars: a large fraction of CEMP-s stars have higher [C/H] values. Hence, the high fraction of the CEMP-s stars among the CEMP turnoff stars could be simply due to this bias in the sample. In other words, one can assume that many additional CEMP-no stars could be included among the turnoff stars of our sample, but they have not yet been identified as CEMP stars.

We comment here on five CEMP stars that have remarkable features in their chemical compositions or stellar parameters.

SDSS J1036+1212 – a CEMP-s star with [Fe/H] $= -3.5$ *and a Spite plateau Li abundance*. This extremely metal-poor turnoff star ($T_{\rm eff} = 5850$ K) exhibits excesses of carbon ([C/Fe] $= +1.5$) and Ba ([Ba/Fe] $= +1.3$). The [Sr/Ba] ratio is very low ([Sr/Ba] $= -2.1$), suggesting the contribution of the s-process even at extremely low metallicity, which efficiently produces heavy elements due to the high ratio of neutrons to seed nuclei (e.g., Busso et al. 1999). The Li I resonance line is clearly detected for this star, even in our snapshot spectrum with a moderate S/N ratio. The equivalent width of the Li line is 52mÅ, resulting in $\log \epsilon$(Li) $= 2.2$. This value agrees with the Li abundances typically found for metal-poor turnoff stars (the so-called Spite plateau value, e.g., Spite & Spite 1982;

Meléndez et al. 2010). The excesses of carbon and barium in such stars is usually interpreted as the result of mass transfer from a companion AGB star. If the amount of mass transferred from the AGB star was large, and the Li was depleted on the surface of the AGB star, the Li should also be depleted in the star we are currently observing. Thus, more accurate determinations of the Li abundance of this star will provide an upper limit on the mass transferred from the AGB star. We have already obtained a higher-S/N spectrum of this object, and a detailed study will appear in a separate paper in this series.

SDSS J1613+5309 – a CEMP-no star with an Mg excess. This object is an EMP ([Fe/H] $= -3.3$) giant that exhibits a moderate excess of Mg ([Mg/Fe] $= +0.9$), but no excess of Ba. Two previously identified CEMP stars are known to possess large excesses of α-elements (CS 22949–037 and CS 29498–043: McWilliam et al. 1995, Aoki et al. 2002a, 2002b), and are referred to as CEMP-α stars (Beers & Christlieb 2005). Although the excess of the α-elements of SDSS J1613+5309 is not as clear as for the two previous objects, this star is likely a new member of the CEMP-α class. We note in passing that enhanced α-elements are often (though not always) associated with the CEMP-no class.

SDSS J1836+6317 and SDSS J1245−0738 – CEMP-s stars with large excesses of Na and Mg. These are typical CEMP-s stars, having [Ba/Fe] $> +2.0$. They exhibit large excesses of Na ([Na/Fe] $> +1.3$) and moderate excesses of Mg ([Mg/Fe] $\sim +0.8$). Similar overabundances of Na and Mg are also found in several previously studied CEMP-s stars, e.g., LP 625–44 (Aoki et al. 2002a). Although the source of the Na and Mg in such objects is not well understood, nucleosynthesis in AGB stars that yielded the large overabundances of neutron-capture elements may also be related to the production of these light elements. For instance, the s-process models by Bisterzo et al. (2011) suggest dependence of Na production by ^{22}Ne$(n, \gamma)^{23}$Ne (and β-decay of ^{23}Ne) on stellar mass.

SDSS J0126+0607 – a "hot" CEMP-s star. The $T_{\rm eff}$ of this object is the highest (6900 K) in our sample, and the excesses of carbon and Ba are also the highest ([C/Fe] $= +3.1$ and [Ba/Fe] $= +3.2$). Such CEMP-s stars could be formed by accretion of significant amounts of carbon-enhanced material from an AGB star across a binary system. Some previously known hot ($T_{\rm eff} \sim 7000$ K) CEMP-s stars (e.g., CS 29497–030: Sivarani et al. 2004, Ivans et al. 2005; CS 29526–110: Aoki et al. 2008) exhibit variations of radial velocities with short timescales (less than one year). Future monitoring of the radial velocity for this object, as well as more detailed chemical-abundance studies, will provide new insight for the formation mechanism of such hot CEMP-s stars.

5.2. *The α-elements*

5.2.1. *Abundance Scatter and Outliers*

Figure 8 shows the abundance ratios of [Mg/Fe], [Ca/Fe], and [Mg/Ca] for turnoff stars (filled circles) and cooler stars (open circles). The average and standard deviation of the abundance ratios for each 0.2 dex bin of [Fe/H] are indicated by large open circles and bars, connected by a solid line. The average and standard deviation of the abundance ratios determined by previous studies, which are taken from the SAGA database (Suda et al. 2008), are also shown by crosses and a dashed line, for comparison. The standard deviations of [Mg/Fe] and [Ca/Fe] of our sample are 0.25–0.35 dex, as small as the

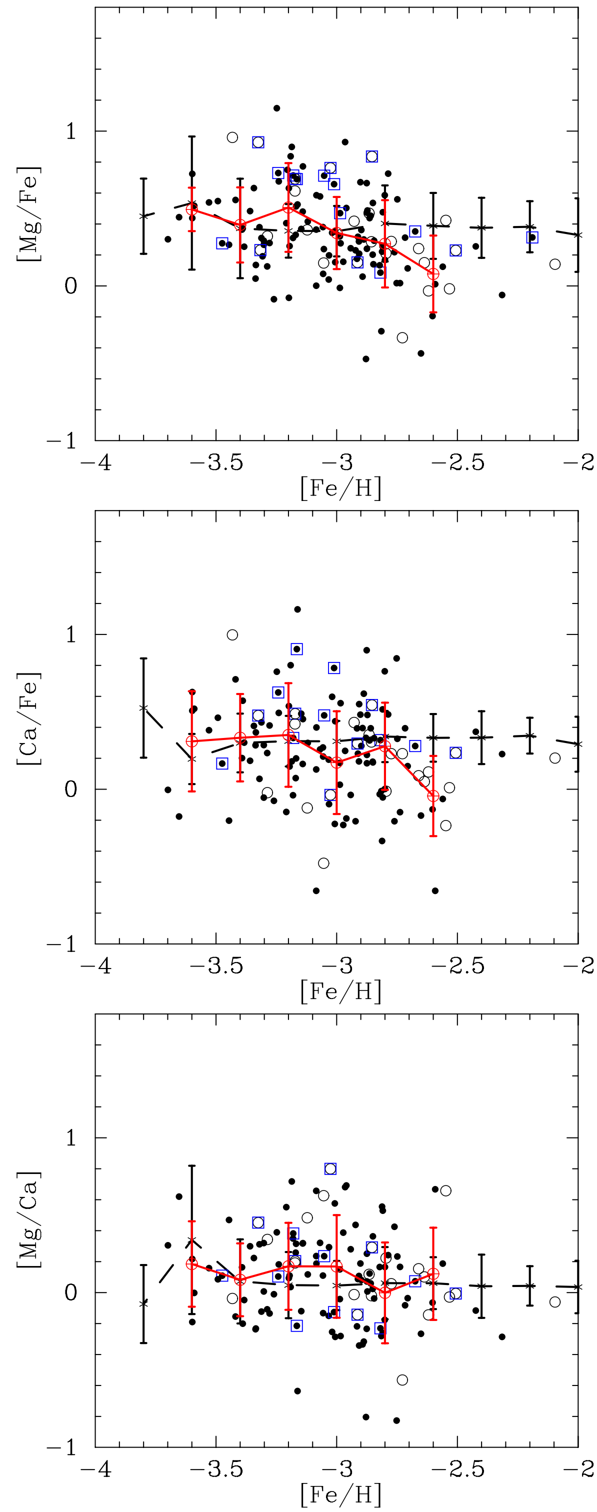

Figure 8. Abundance ratios of [Mg/Fe] (top panel), [Ca/Fe] (middle panel), and [Mg/Ca] (bottom panel), with respect to [Fe/H]. The filled and open circles indicate main-sequence turnoff and giant stars, respectively. CEMP stars ([C/Fe] $> +0.7$) are shown by overplotting open squares. Large open circles and bars, connected by a solid line (red), represent the average and standard deviation of the abundance ratios, respectively, for each metallicity bin of width 0.2 dex for our SDSS sample. The standard deviations are 0.20–0.25 dex, which are as small as the random errors in the abundance measurements. Crosses and bars, connected by a dashed line, indicate those for the SAGA sample (see the text).

(A color version of this figure is available in the online journal.)

measurement errors. Hence, no clear intrinsic scatter of the abundance ratios is found in these diagrams.

Non-LTE effects on abundance measurements for extremely metal-poor stars were investigated for Mg by Andrievsky et al. (2010), and for Ca by Mashonkina et al. (2007) and Spite et al. (2012). The non-LTE corrections for Mg are positive, and the size is 0.1–0.3 dex, according to Andrievsky et al. (2010). The corrections are systematically larger for dwarf stars than for giants. Hence, the Mg abundance ratios could be systematically higher than those derived by our LTE analysis. The non-LTE corrections for Ca abundances measured from neutral species are dependent on spectral lines: the correction is largest for measurements based on the Ca I 4226 Å line, which is used in our analysis for a portion of the sample. The corrections are estimated to be 0.0–0.2 dex by Spite et al. (2012). Hence, the effects are not significant when other lines (such as the subordinate lines) of Ca I are available, as in the case of analyses for giants in our sample. We note that the abundance results taken from the SAGA database are based on LTE analyses.

We would like to comment on possible outliers in Mg abundances as candidate α-element-enhanced or α-deficient stars. Although some apparent outliers exist in [Ca/Fe], the Ca abundances are determined from only one feature at 4226 Å in many cases, for which the S/N ratios are not as high as in the red range, and which could be affected by contamination from the CH features in carbon-enhanced objects. Hence, the Ca abundances are discussed only for comparison purposes.

There are seven stars that have [Mg/Fe] $>$ +0.8. Two of them are CEMP stars, as discussed above. Three objects (SDSS J0840+5405, SDSS J1623+3913, and SDSS J2104−0104) also exhibit some excess of Ca ([Ca/Fe] $>$ +0.7), suggesting that their excesses of the α-elements are real.

The Mg abundance ratios of the other two stars (SDSS J1412+5609 and SDSS J1424+5615) are also very high ([Mg/Fe] $\sim$ +0.9), while their Ca abundances appear normal. If this result is real, this suggests scatter of chemical-abundance ratios produced by the progenitor massive star and its supernova explosion.

There are four stars that have [Mg/Fe] $<$ −0.2. One of the four stars is a cool main-sequence star (SDSS J0018−0939: [Mg/Fe] = −0.44). The Mg abundance is determined from the Mg I b lines, which are rather sensitive to the adopted broadening parameter. However, the non-detection of other Mg I lines (e.g., 5528 Å) results in an upper limit of [Mg/Fe] $\sim$ 0.0, indicating a deficiency of Mg in this star. The [Ca/Fe] ratio of this star is also below the solar value. Moreover, the carbon abundance of this object is very low ([C/Fe] = −0.7), as mentioned in Section 4.4. The Na is also significantly underabundant ([Na/Fe] = −1.0). Further detailed abundance study of this object is desirable, as a candidate VMP star revealing a peculiar nucleosynthesis episode in the early chemical enrichment of the Galaxy.

Another object (SDSS J0254+3328: [Mg/Fe] = −0.3) also exhibits a relatively low Ca abundance ([Ca/Fe] = 0.0) for a star at this very low metallicity ([Fe/H] = −2.8), and could be an α-element-deficient star. The other two stars, SDSS J1241−0837 and SDSS J1633+3907, have normal Ca abundances for halo stars, and the deficiency of the α-elements in general is unclear.

Excluding such outliers, no clear scatter of the [α/Fe] ratios is detected, within the measurement errors, in our sample. This indicates that there is no large scatter in the abundance ratios of these elements even at very low metallicity, as suggested by previous studies (François et al. 2004; Arnone et al. 2005; Andrievsky et al. 2010). Higher quality spectra are required to investigate the small size of the abundance scatter, if any, which will provide useful constraints on the early chemical enrichment of the Galaxy by supernovae and subsequent mixing in the interstellar medium.

5.2.2. Abundance Trends

The averages of [Mg/Fe] and [Ca/Fe] clearly exhibit overabundances of these elements in EMP stars, as have been found by numerous previous studies (e.g., Ryan et al. 1996; McWilliam 1997; Cayrel et al. 2004). There is no clear increasing or decreasing trend of the [Mg/Fe] and [Ca/Fe] abundance ratios in the sample taken from the SAGA database, as shown by the dashed lines in Figure 8. This is also the case for stars with [Fe/H] $\leqslant -2.8$ in our sample; the average values of [Mg/Fe] and [Ca/Fe] are +0.4 and +0.3, respectively, in agreement with those reported by many previous studies (e.g., Lai et al. 2008; Andrievsky et al. 2010).

However, the abundance ratios at [Fe/H] $= -2.6$ ($\langle$[Mg/Fe]$\rangle$ = +0.08 and $\langle$[Ca/Fe]$\rangle$ = −0.04) are lower than these averages for the stars with [Fe/H] < -2.8. Although the standard deviations are as large as 0.25 dex, the difference is statistically significant, given the sample size (11 objects) in this bin. Indeed, the null hypothesis that the [Mg/Fe] for stars in the bin ($-2.7 <$ [Fe/H] $\leqslant -2.5$) and for the lower metallicity stars ([Fe/H] $\leqslant -2.7$) are drawn from the same parent population is rejected by the Mann-Whitney rank-sum test at high significance ($p < 0.001$).

This metallicity bin includes a relatively large fraction of giants (six giants among the 11 stars). However, there is no significant difference in the average [Mg/Fe] between giants and turnoff stars in our entire sample (the difference is less than 0.01 dex). Moreover, the average [Mg/Fe] for the six giants in the metallicity range $-2.7 <$ [Fe/H] $\leqslant -2.5$ ($\langle$[Mg/Fe]$\rangle$ = +0.16) is rather higher than for the five turnoff stars in the bin ($\langle$[Mg/Fe]$\rangle$ = −0.03). Hence, the relatively large fraction of giants in this bin is unlikely to be the reason for the low [Mg/Fe].

The [Mg/Ca] ratio is almost constant over the full metallicity range in our sample, as found by previous studies. Hence, the abundance trend of our sample suggests a decreasing trend of the α-elements at [Fe/H] ~ -2.5.

Recent abundance studies of halo stars with available full space motions suggest different trends in the [α/Fe] abundance ratios depending on kinematics (Zhang et al. 2009; Ishigaki et al. 2010; Nissen & Schuster 2010). These studies mostly include less metal-poor stars ([Fe/H] $\gtrsim -2.0$) than our sample. Further investigations of the kinematics, as well as their chemical abundance ratios, for significantly more metal-poor stars, such as those included in our present sample, is desired to understand the early formation processes of the Galactic halo system.

5.3. Sr and Ba

Figure 9 shows the abundance ratios of [Sr/Fe], [Ba/Fe], and [Sr/Ba] as a function of metallicity. The results are compared with those obtained by previous studies, also taken from the SAGA database (Suda et al. 2008), which are shown by open circles (carbon-normal stars) and asterisks (carbon-enhanced stars).

Non-LTE effects on Sr and Ba abundance determinations were investigated by Andrievsky et al. (2011) and Andrievsky et al. (2009), respectively. The abundance corrections for Ba are positive, hence our LTE analyses could systematically

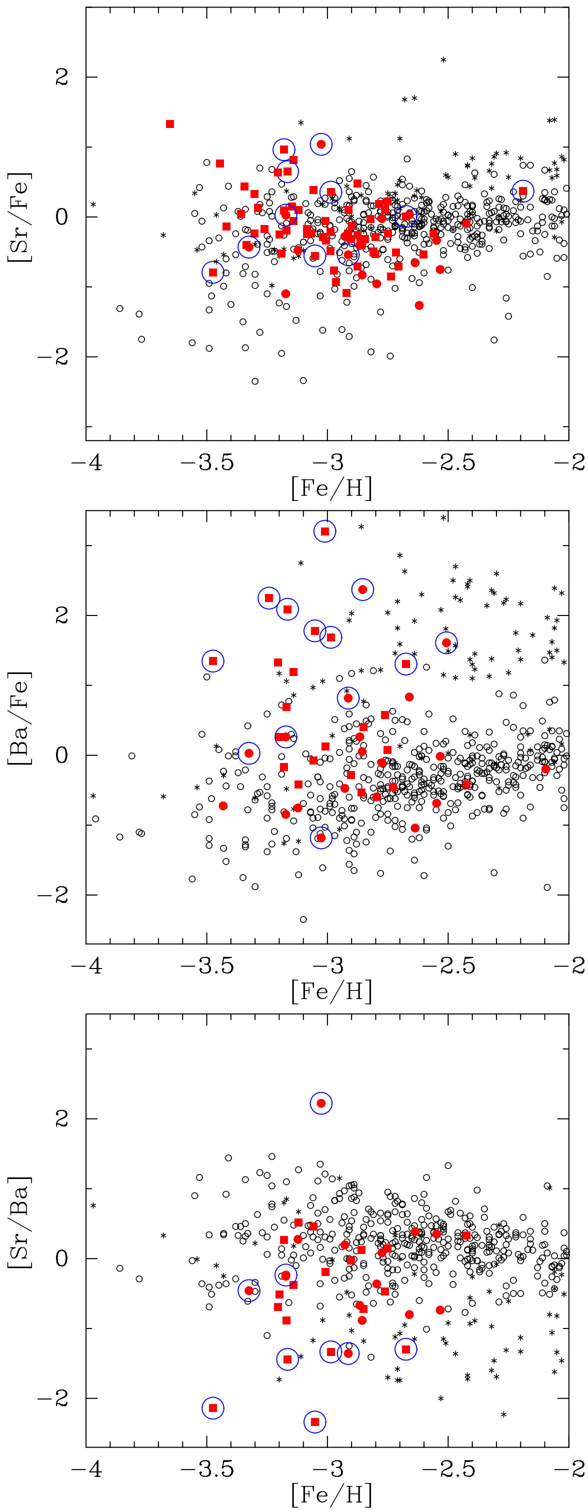

Figure 9. Abundance ratios of neutron-capture elements ([Sr/Fe], [Ba/Fe], and [Sr/Ba]) as a function of [Fe/H]. The filled squares and circles (red) indicate main-sequence turnoff and giant stars, respectively. CEMP stars ([C/Fe] > +0.7) are overplotted by large open circles (blue). Small open circles and asterisks indicate the abundance ratios of carbon-normal and carbon-rich stars, respectively, measured by previous studies, which are taken from the SAGA database.

(A color version of this figure is available in the online journal.)

underestimate the Ba abundances, though the correction would be at most 0.3 dex. The correction for Sr abundances determined from the Sr II 4077 and 4215 Å lines could be positive and negative, depending on the stellar parameters. The corrections are, however, at most 0.2 dex. Since these effects are much smaller than the scatter found in the Sr and Ba abundance ratios, our discussion here is not significantly affected by the non-LTE effects.

The [Sr/Fe] ratios (top panel) exhibit a scatter of about one order of magnitude. Interestingly, this scatter is much *smaller* than that found by previous studies at $[Fe/H] \sim -3$ (e.g., McWilliam et al. 1995; Ryan et al. 1996; Honda et al. 2004; Aoki et al. 2005; François et al. 2007). However, this could be the result of a bias in the sample, since the Sr II lines are in the blue range (where the spectral data quality is not high), and are only detected in stars having high Sr abundance. Indeed, the objects in our sample distribute in the range of $[Sr/Fe] \gtrsim -1$, below which many stars are found in the SAGA sample. In other words, there are likely to be many stars having lower [Sr/Fe] ratios in our sample for which the Sr lines are not detected.

Although the situation is similar for the [Ba/Fe] ratios (middle panel), the scatter is much larger than for [Sr/Fe]. This is mostly due to the large excesses of Ba in carbon-enhanced stars (the CEMP-s stars), which are shown by overplotting large open circles. This is clear from the comparison with previous studies: carbon-enhanced objects in the SAGA sample are shown by asterisks in Figure 9. The s-process at low metallicity is known to yield larger amounts of heavy neutron-capture elements, such as Ba, compared to lighter elements such as Sr (e.g., Busso et al. 1999; Bisterzo et al. 2011). This is clearly seen in the [Sr/Ba] ratios (bottom panel), where most of the CEMP stars exhibit low [Sr/Ba] ratios. There is one exception, at $[Fe/H] = -3.0$, that has a very high [Sr/Ba] ratio ($[Sr/Ba] = +2.2$). This star, SDSS J1422+0031, exhibits no excess of Ba ($[Ba/Fe] = -1.0$), and is classified as a CEMP-no star.

Excluding the CEMP-s stars, four other stars have $[Ba/Fe] > +0.5$. Among them, SDSS J2357–0052 is a highly r-process-enhanced (r-II) star, reported on in detail by Aoki et al. (2010). This object is the first example of a cool EMP main-sequence star with large excesses of r-process elements. The metallicity is the lowest, and the excess of Eu is the highest ($[Eu/Fe] = +1.9$), among the r-II stars known to date. We note that the Fe abundance of this object derived in the present work ($[Fe/H] = -3.2$) is slightly higher than the result of Aoki et al. (2010), because the $T_{\rm eff}$ adopted here is slightly higher.

SDSS J0932+0241 is another EMP star exhibiting a large excess of Ba ($[Ba/Fe] = +1.2$). Because of the limited quality of our spectrum and the star's high temperature ($T_{\rm eff} = 6200$ K), the abundances of most other heavy elements are not determined. We note that the [Sr/Ba] ratio of this star ($[Sr/Ba] = -0.3$) is significantly higher than the values found in CEMP-s stars, suggesting the origin of these heavy elements are attributable to the r-process, rather than to the s-process. If this is confirmed, this object is the first clear example of r-II stars at the main-sequence turnoff (Sneden et al. 2008). Further detailed abundance study is desirable for this object to firmly establish the origin of the excess in Ba.

The other two stars, SDSS J0008–0529 and SDSS J2128–0756, exhibit [Ba/Fe] ratios of +0.6 and +0.8, respectively. If the origin of the Ba in these stars is the r-process, the [Eu/Fe] values are expected to be higher than +1. Measurements of the heavy elements in these objects, based on higher quality spectra, are also desirable for further studies of r-II stars.

Another interesting object is SDSS J0140+2344, which has a large overabundance of Sr ($[Sr/Fe] > +1$) with no clear excess of Ba. Though many metal-poor stars having high Sr/Ba ratios are known (e.g., Honda et al. 2004; François et al. 2007), this object is unique because of its low metallicity ([Fe/H] = −3.7). Further detailed abundance study is desired to understand the implication of the Sr overabundance in this object.

6. SUMMARY

We have determined stellar parameters and chemical compositions, based on high-resolution spectra obtained with the Subaru/HDS, for 137 very/extremely metal-poor stars selected from SDSS/SEGUE. Comparisons of the Fe abundances derived by the present work with the estimates by the recent pipeline analyses for the SDSS spectra (SSPP) exhibit no significant offset, even in the lowest metallicity range ([Fe/H] $<$ −3), while scatter in the comparisons indicates that high-resolution spectroscopy is required to determine accurate metallicity for individual stars. The abundance ratios of carbon, the α-elements, and the neutron-capture elements derived from our high-resolution spectra will provide useful calibrations for the estimates from SDSS spectra.

The fraction of carbon-enhanced objects and the abundance ratios of α-elements and neutron-capture elements are discussed for the overall sample. More detailed abundance patterns will be studied based on higher-resolution, higher-S/N spectra for selected objects, in particular those having the lowest metallicity ([Fe/H] $\lesssim -3.5$).

Our sample includes three double-lined spectroscopic binaries (including a triple system), for which chemical compositions of the primary stars are estimated taking the veiling by the secondary into consideration. Follow-up studies for these binaries will be useful for understanding low-mass star formation at low metallicity in the early era of the Galaxy.

Funding for the SDSS and SDSS-II has been provided by the Alfred P. Sloan Foundation, the Participating Institutions, the National Science Foundation, the U.S. Department of Energy, the National Aeronautics and Space Administration, the Japanese Monbukagakusho, the Max Planck Society, and the Higher Education Funding Council for England. The SDSS Web site is http://www.sdss.org/.

The SDSS is managed by the Astrophysical Research Consortium for the Participating Institutions. The Participating Institutions are the American Museum of Natural History, Astrophysical Institute Potsdam, University of Basel, Cambridge University, Case Western Reserve University, University of Chicago, Drexel University, Fermilab, the Institute for Advanced Study, the Japan Participation Group, Johns Hopkins University, the Joint Institute for Nuclear Astrophysics, the Kavli Institute for Particle Astrophysics and Cosmology, the Korean Scientist Group, the Chinese Academy of Sciences (LAMOST), Los Alamos National Laboratory, the Max-Planck-Institute for Astronomy (MPIA), the Max-Planck-Institute for Astrophysics (MPA), New Mexico State University, Ohio State University, University of Pittsburgh, University of Portsmouth, Princeton University, the United States Naval Observatory, and the University of Washington.

W.A. was supported by the JSPS Grants-in-Aid for Scientific Research (23224004). T.C.B. and Y.S.L. acknowledge partial funding of this work from grants PHY 02-16783 and PHY 08-22648: Physics Frontier Center/Joint Institute for Nuclear Astrophysics (JINA), awarded by the U.S. National Science Foundation. M.T.-H. is grateful for a support by the JSPS Grants-in-Aid for Scientific Research (22540255).

Facilities: Sloan, Subaru

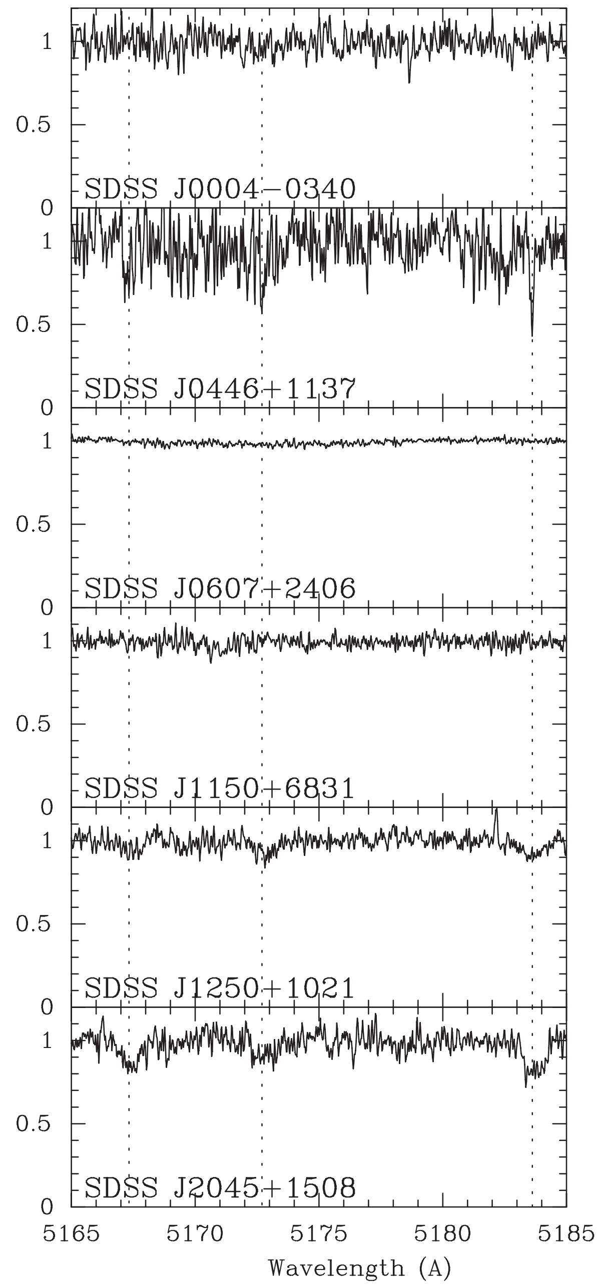

Figure 10. Spectra of objects not analyzed in the present work, in the region of the Mg I b lines. The line positions of the triplet are shown by vertical dotted lines.

APPENDIX

OBJECTS NOT ANALYZED

The six objects observed, but not analyzed, in the present work are listed in Table 8. The spectra around the wavelengths of Mg I b lines and Hα are shown in Figures 10 and 11.

Two objects (SDSS J0004−0340 and SDSS J1150 + 6831) are included in the list of white dwarfs reported by Debes et al. (2011). They exhibit broad and shallow Hα absorption lines and no clear Mg I b lines (Figures 10 and 11). SDSS J1250 + 1021 and SDSS J2045 + 1508 also show broad or shallow Hα absorption features with weak Mg I b lines. They could be relatively cool white dwarfs, though further confirmation is required.

Table 8
List of Objects Not Analyzed

ID	Object	Object Name	Object ID	g_0	$(g-r)_0$	V_0	Remarks
U1	SDSS J0004−0340	SDSS J000410.42−034008.6	2624-54380-458	16.762	0.131	16.685	LP 644–30, WD[a]
U2	SDSS J0446 + 1137	SDSS J044655.70 + 113741.3	2669-54086-593	16.376	0.248	16.232	
U3	SDSS J0607 + 2406	SDSS J060740.48 + 240651.3	2887-54521-537	13.690	0.470	13.422	close to NGC 2168
U4	SDSS J1150 + 6831	SDSS J115052.32 + 683116.1	0492-51955-523	15.337	0.230	15.204	WD[a]
U5	SDSS J1250 + 1021	SDSS J125005.10 + 102156.4	2963-54589-474	16.276	0.257	16.128	
U6	SDSS J2045 + 1508	SDSS J204524.04 + 150825.5	2250-53566-249	16.358	0.441	16.107	

Note. [a] White dwarfs listed by Debes et al. (2011).

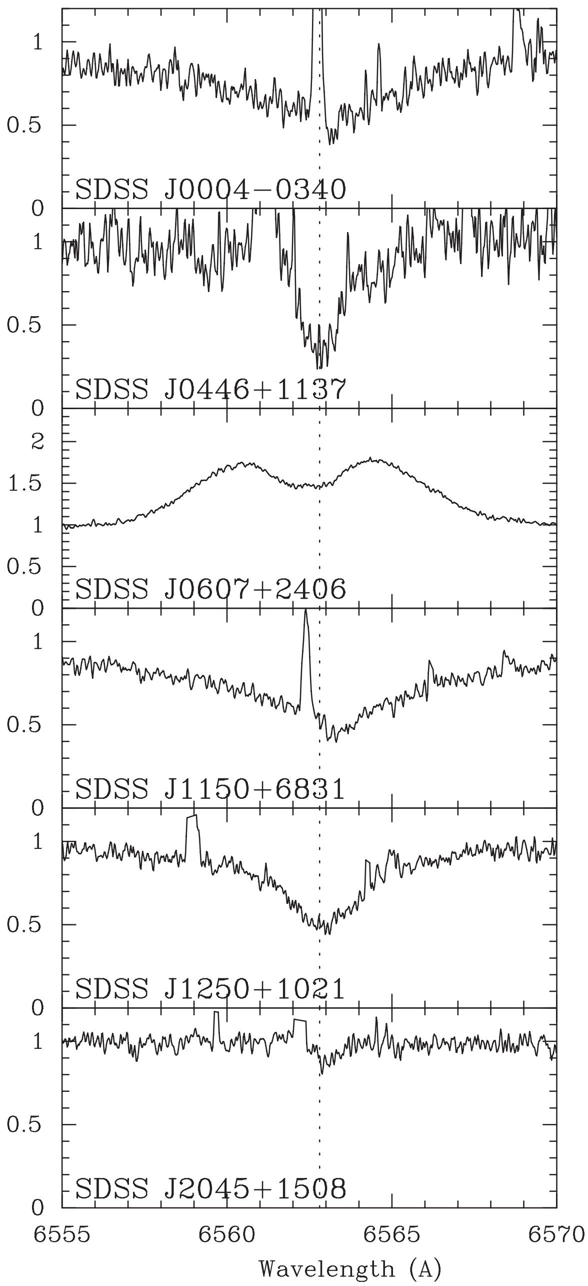

Figure 11. Same as Figure 10, but for the Hα region. The line position is shown by a vertical dotted line. Sky emission features are not fully removed in this region.

SDSS J0607 + 2406 is a bright object, but exhibits an emission feature of Hα, and is clearly not a normal metal-poor star. This object is close to the cluster NGC 2168, and identification with objects reported by previous studies is not straightforward.

SDSS J0446+1137 is likely a metal-poor star, though the S/N ratio of the current spectrum is not sufficient for abundance analyses.

REFERENCES

Abazajian, K. N., Adelman-McCarthy, J. K., Agüeros, M. A., et al. 2009, ApJS, 182, 543
Aldenius, M., Tanner, J. D., Johansson, S., Lundberg, H., & Ryan, S. G. 2007, A&A, 461, 767
Allende Prieto, C., Sivarani, T., Beers, T. C., et al. 2008, AJ, 136, 2070
Alonso, A., Arribas, S., & Martínez-Roger, C. 1999, A&AS, 140, 261
Andrievsky, S. M., Spite, M., Korotin, S. A., et al. 2009, A&A, 494, 1083
Andrievsky, S. M., Spite, M., Korotin, S. A., et al. 2010, A&A, 509, A88
Andrievsky, S. M., Spite, F., Korotin, S. A., et al. 2011, A&A, 530, A105
Aoki, W., Barklem, P. S., Beers, T. C., et al. 2009, ApJ, 698, 1803
Aoki, W., Beers, T. C., Christlieb, N., et al. 2007, ApJ, 655, 492
Aoki, W., Beers, T. C., Honda, S., & Carollo, D. 2010, ApJ, 723, L201
Aoki, W., Beers, T. C., Sivarani, T., et al. 2008, ApJ, 678, 1351
Aoki, W., Frebel, A., Christlieb, N., et al. 2006, ApJ, 639, 897
Aoki, W., Honda, S., Beers, T. C., et al. 2005, ApJ, 632, 611
Aoki, W., Norris, J. E., Ryan, S. G., Beers, T. C., & Ando, H. 2002a, PASJ, 54, 427
Aoki, W., Norris, J. E., Ryan, S. G., Beers, T. C., & Ando, H. 2002b, ApJ, 576, L141
Arnone, E., Ryan, S. G., Argast, D., Norris, J. E., & Beers, T. C. 2005, A&A, 430, 507
Asplund, M., Grevesse, N., Sauval, A. J., & Scott, P. 2009, ARA&A, 47, 481
Barklem, P. S., Christlieb, N., Beers, T. C., et al. 2005, A&A, 439, 129
Beers, T. C., & Christlieb, N. 2005, ARA&A, 43, 531
Beers, T. C., Preston, G. W., & Shectman, S. A. 1985, AJ, 90, 2089
Beers, T. C., Preston, G. W., & Shectman, S. A. 1992, AJ, 103, 1987
Bessell, M. S., & Norris, J. 1984, ApJ, 285, 622
Biemont, E., Baudoux, M., Kurucz, R. L., Ansbacher, W., & Pinnington, E. H. 1991, A&A, 249, 539
Biemont, E., & Godefroid, M. 1980, A&A, 84, 361
Bisterzo, S., Gallino, R., Straniero, O., Cristallo, S., & Käppeler, F. 2011, MNRAS, 418, 284
Blackwell, D. E., Menon, S. L. R., Petford, A. D., & Shallis, M. J. 1982a, MNRAS, 201, 611
Blackwell, D. E., Petford, A. D., Shallis, M. J., & Leggett, S. 1982b, MNRAS, 199, 21
Bonifacio, P., Sbordone, L., Caffau, E., et al. 2012, A&A, 542, A87
Bonifacio, P., Spite, M., Cayrel, R., et al. 2009, A&A, 501, 519
Booth, A. J., Blackwell, D. E., Petford, A. D., & Shallis, M. J. 1984, Obs, 104, 265
Bromm, V., & Larson, R. B. 2004, ARA&A, 42, 79
Busso, M., Gallino, R., & Wasserburg, G. J. 1999, ARA&A, 37, 239
Caffau, E., Bonifacio, P., François, P., et al. 2011, Natur, 477, 67
Carollo, D., Beers, T. C., Bovy, J., et al. 2012, ApJ, 744, 195
Casagrande, L., Ramírez, I., Meléndez, J., Bessell, M., & Asplund, M. 2010, A&A, 512, A54
Castelli, F., & Kurucz, R. L. 2003, Modelling Stellar Atmos, 210, 20P
Cayrel, R., Depagne, E., Spite, M., et al. 2004, A&A, 416, 1117
Christlieb, N. 2003, RvMA, 16, 191
Christlieb, N., Bessell, M. S., Beers, T. C., et al. 2002, Natur, 419, 904
Christlieb, N., Schörck, T., Frebel, A., et al. 2008, A&A, 484, 721
Ciardi, B., & Ferrara, A. 2005, SSRv, 116, 625
Cohen, J. G., Christlieb, N., McWilliam, A., et al. 2004, ApJ, 612, 1107
Cooke, R., Pettini, M., Steidel, C. C., Rudie, G. C., & Jorgenson, R. A. 2011, MNRAS, 412, 1047

Debes, J. H., Hoard, D. W., Wachter, S., Leisawitz, D. T., & Cohen, M. 2011, ApJS, 197, 38
Demarque, P., Woo, J.-H., Kim, Y.-C., & Yi, S. K. 2004, ApJS, 155, 667
Fischer, F. C. 1975, CaJPh, 53, 189
François, P., Depagne, E., Hill, V., et al. 2007, A&A, 476, 935
François, P., Matteucci, F., Cayrel, R., et al. 2004, A&A, 421, 613
Frebel, A., Aoki, W., Christlieb, N., et al. 2005, Natur, 434, 871
Frebel, A., & Norris, J. E. 2011, arXiv:1102.1748
Gallagher, A. 1967, PhRv, 157, 24
Goldberg, D., Mazeh, T., Latham, D. W., et al. 2002, AJ, 124, 1132
Gunn, J. E., Siegmund, W. A., Mannery, E. J., et al. 2006, AJ, 131, 2332
Hannaford, P., Lowe, R. M., Grevesse, N., Biemont, E., & Whaling, W. 1982, ApJ, 261, 736
Hirschi, R., Frölich, C., Liebendorfer, M., & Thilemann, F.-K. 2006, RvMA, 19, 101
Hollek, J. K., Frebel, A., Roederer, I. U., et al. 2011, ApJ, 742, 54
Honda, S., Aoki, W., Kajino, T., et al. 2004, ApJ, 607, 474
Ishigaki, M., Chiba, M., & Aoki, W. 2010, PASJ, 62, 1369
Ito, H., Aoki, W., Honda, S., & Beers, T. C. 2009, ApJ, 698, L37
Ivans, I. I., Simmerer, J., Sneden, C., et al. 2006, ApJ, 645, 613
Ivans, I. I., Sneden, C., Gallino, R., Cowan, J. J., & Preston, G. W. 2005, ApJ, 627, L145
Kim, Y.-C., Demarque, P., Yi, S. K., & Alexander, D. R. 2002, ApJS, 143, 499
Kobayashi, C., Tominaga, N., & Nomoto, K. 2011, ApJ, 730, L14
Kupka, F., Piskunov, N., Ryabchikova, T. A., Stempels, H. C., & Weiss, W. W. 1999, A&AS, 138, 119
Kurucz, R. 1993, ATLAS9 Stellar Atmosphere Programs and 2 km/s Grid, Kurucz CD-ROM No. 13 (Cambridge, MA: Smithsonian Astrophysical Observatory)
Lai, D. K., Bolte, M., Johnson, J. A., et al. 2008, ApJ, 681, 1524
Lawler, J. E., Bonvallet, G., & Sneden, C. 2001a, ApJ, 556, 452
Lawler, J. E., & Dakin, J. T. 1989, JOSAB, 6, 1457
Lawler, J. E., Wickliffe, M. E., den Hartog, E. A., & Sneden, C. 2001b, ApJ, 563, 1075
Lee, Y. S., Beers, T. C., Allende Prieto, C., et al. 2011, AJ, 141, 90
Lee, Y. S., Beers, T. C., Sivarani, T., et al. 2008a, AJ, 136, 2022
Lee, Y. S., Beers, T. C., Sivarani, T., et al. 2008b, AJ, 136, 2050
Martin, G. A., Fuhr, J. R., & Wiese, W. L. 1988, Atomic Transition Probabilities. Scandium through Manganese (New York: American Institute of Physics (AIP) and American Chemical Society)
Mashonkina, L., Korn, A. J., & Przybilla, N. 2007, A&A, 461, 261
McWilliam, A. 1997, ARA&A, 35, 503
McWilliam, A., Preston, G. W., Sneden, C., & Searle, L. 1995, AJ, 109, 2757
Meléndez, J., Casagrande, L., Ramírez, I., Asplund, M., & Schuster, W. J. 2010, A&A, 515, L3
Meynet, G., Ekström, S., & Maeder, A. 2006, A&A, 447, 623
Meynet, G., Hirschi, R., Ekström, S., et al. 2010a, in IAU Symp. 265, Chemical Abundances in the Universe: Connecting First Stars to Planets (Cambridge: Cambridge Univ. Press), 98
Meynet, G., Hirschi, R., Ekström, S., et al. 2010b, A&A, 521, A30
Moity, J. 1983, A&AS, 52, 37
Nissen, P. E., & Schuster, W. J. 2010, A&A, 511, L10
Nitz, D. E., Kunau, A. E., Wilson, K. L., & Lentz, L. R. 1999, ApJS, 122, 557
Noguchi, K., Aoki, W., Kawanomoto, S., et al. 2002, PASJ, 54, 855
Norris, J. E., Bessell, M. S., Yong, D., et al. 2012, ApJ, in press (arXiv:1208.2999)
Norris, J. E., Christlieb, N., Korn, A. J., et al. 2007, ApJ, 670, 774
O'Brian, T. R., Wickliffe, M. E., Lawler, J. E., Whaling, W., & Brault, J. W. 1991, JOSAB, 8, 1185
Pickering, J. C., Thorne, A. P., & Perez, R. 2001, ApJS, 132, 403
Pinnington, E. H., Berends, R. W., & Lumsden, M. 1995, JPhB, 28, 2095
Press, W. H., Teukolsky, S. A., Vetterling, W. T., & Flannery, B. P. 1992, Numerical Recipes in FORTRAN. The Art of Scientific Computing (2nd ed.; Cambridge: Cambridge Univ. Press)
Ryabchikova, T. A., Hill, G. M., Landstreet, J. D., Piskunov, N., & Sigut, T. A. A. 1994, MNRAS, 267, 697
Ryan, S. G., Norris, J. E., & Beers, T. C. 1996, ApJ, 471, 254
Schlegel, D., Finkbeiner, D., & Davis, M. 1998, ApJ, 500, 525
Schnabel, R., Schultz-Johanning, M., & Kock, M. 2004, A&A, 414, 1169
Sivarani, T., Bonifacio, P., Molaro, P., et al. 2004, A&A, 413, 1073
Skrutskie, M. F., Cutri, R. M., Stiening, R., et al. 2006, AJ, 131, 1163
Smolinski, J. P., Lee, Y. S., Beers, T. C., et al. 2011, AJ, 141, 89
Sneden, C., Cowan, J. J., & Gallino, R. 2008, ARA&A, 46, 241
Spite, M., Andrievsky, S. M., Spite, F., et al. 2012, A&A, 541, A143
Spite, F., & Spite, M. 1982, A&A, 115, 357
Suda, T., Aikawa, M., Machida, M. N., Fujimoto, M. Y., & Iben, I., Jr. 2004, ApJ, 611, 476
Suda, T., Katsuta, Y., Yamada, S., et al. 2008, PASJ, 60, 1159
Tominaga, N., Umeda, H., & Nomoto, K. 2007, ApJ, 660, 516
Tsuji, T. 1978, A&A, 62, 29
Umeda, H., & Nomoto, K. 2003, Natur, 422, 871
Umeda, H., & Nomoto, K. 2005, ApJ, 619, 427
Wiese, W. L., & Martin, G. A. 1980, NSRDS-NBS, 68
Wiese, W. L., Smith, M. W., & Miles, B. M. 1969, NSRDS-NBS (Washington, DC: US Department of Commerce, National Bureau of Standards)
Yanny, B., Rockosi, C., Newberg, H. J., et al. 2009, AJ, 137, 4377
Yong, D., Norris, J. E., Bessell, M. S., et al. 2012, ApJ, in press (arXiv:1208.3003)
York, D. G., Adelman, J., Anderson, J. E., Jr., et al. 2000, AJ, 120, 1579
Zhang, L., Ishigaki, M., Aoki, W., Zhao, G., & Chiba, M. 2009, ApJ, 706, 1095
Zhao, C., & Newberg, H. J. 2006, arXiv:astro-ph/0612034